Implication of Terrain Topology Modelling on Ground Vehicle Reliability

Sujay J. Kawale

Thesis submitted to the faculty of the Virginia Polytechnic Institute and State University

in partial fulfillment of the requirements for the degree of

Master of Science

In

Mechanical Engineering

John B. Ferris

Robert L. West

Saied Taheri

February 2nd, 2011

Blacksburg, Virginia

Keywords: terrain modelling, autoregressive, Markov chain, fatigue analysis, durability

Implication of Terrain Topology Modelling on Ground Vehicle Reliability

Sujay J. Kawale

Abstract

The accuracy of computer-based ground vehicle durability and ride quality simulations depends on accurate representation of road surface topology as an excitation to vehicle dynamics simulation software, since most of the excitation input to a vehicle as it traverses terrain is provided by the surface topology. It is not computationally efficient to utilise physically measured terrain topology for these simulations since extremely large data sets would be required to represent terrain of all desired types. Moreover, performing repeated simulations on the same set of measured data would not provide a random character typical of real world usage.

There exist several methods of synthesising terrain data through the use of stochastic or mathematical models in order to capture such physical properties of measured terrain as roughness, bank angle and grade. In first part of this work, the autoregressive model and the Markov chain model have been applied to generate synthetic two-dimensional terrain profiles. The synthesised terrain profiles generated are expected to capture the statistical properties of the measured data. A methodology is then proposed; to assess the performance of these models of terrain in capturing the statistical properties of the measured terrain. This is done through the application of several statistical property tests to the measured and synthesized terrain profiles.

The second part of this work describes the procedure that has been followed to assess the performance of these models in capturing the vehicle component fatigue-inducing characteristics of the measured terrain, by predicting suspension component fatigue life based on the loading conditions obtained from the measured terrain and the corresponding synthesized terrain. The terrain model assessment methodology presented in this work can be applied to any model of terrain, serving to identify which terrain models are suited to which type of terrain.

Dedication

To Savitri

whose love knows no bounds of any conventional relationships.

Acknowledgements

I would like to take this opportunity to express my sincere gratitude to my advisor, Dr. John Ferris for his guidance and support throughout my research. There is so much I have learned while working with him, and his role in ensuring that I get the best opportunities and exposure is highly appreciated.

I would also like to thank my committee members, Dr. Saied Taheri and Dr. Robert West for their inspiration and guidance, as well as everyone at the Institute for Advanced Learning and Research and Virginia Tech for the role they played during my time in Virginia. Special thanks are in order for my fellow graduate students at the IALR for all the fun times we've had.

I'd also like to thank my parents for all they have done for me, for all their love, support, freedom and sacrifices. Many thanks to my brother Akshay, for his role in my education and recreation. And lastly, Savitri, for her unwavering love and belief in my abilities.

Contents

List of Figures

List of Tables

Nomenclature

A	–	no. of reverse arrangements
a	–	acceleration
a_k	–	AR residual
b,c	–	fatigue strength and ductility exponents
b_i	–	series of constants
b_{ij}	–	series of constants
C	–	characteristic matrix
c	–	normalised damping ratio
C(α)	–	coefficient for calculating D_N^*
c_s	–	damping ratio
D	–	fatigue damage
D_N	–	supremum difference between ECDF and standard normal CDF
D_N^*	–	critical value of D_N
e	–	nominal strain
E	–	Young's modulus
F	–	force, Keenan's test statistic for linearity
G-value	–	statistical goodness-of-fit between two profiles
i	–	initial state of Markov process
IRI	–	International Roughness Index
j	–	final state of Markov process
K	–	stiffness matrix
k	–	terrain profile point under consideration
k_1, k_2	–	normalised spring stiffness
k_s	–	spring stiffness
K_t	–	theoretical stress concentration factor
k_t	–	tire stiffness
K_ε	–	true strain concentration factor
K_σ	–	true stress concentration factor
l	–	correlation length
L	–	length of the profile in meters

m	–	mass
M	–	order of AR model
m_s	–	sprung mass
m_u	–	unsprung mass
N	–	shape function for interpolation
N_f	–	reversals to failure (= ½ of cycles to failure)
P	–	load
p, p-value	–	probability from KS test
p_{ti}	–	probability of time average of signal exceeding the current elevation value
S	–	nominal stress, number of states in Markov chain
S_{max}	–	highest number of states in Markov chain
u	–	displacement vector
V	–	velocity of the quarter car model in m/s
X	–	stationary time series
Z	–	random variable representing terrain elevation value
$\hat{Z}$	–	normalised terrain elevation values
$\dot{z}_s$	–	vertical velocity of the sprung mass
$\dot{z}_u$	–	vertical velocity of the unsprung mass
z_k	–	terrain elevation value
z_{res}	–	resolution of measurement
δW	–	work done

Greek Symbols

α	–	confidence value
δr	–	distance moved by force
ε	–	strain, true strain
ε_e	–	elastic strain
ε_p	–	plastic strain
ε_t	–	total strain (sum of elastic and plastic)
$\hat{\varepsilon}_t$	–	residuals in regression analysis
ε_f'	–	fatigue ductility coefficient

ϵ_t	–	random series
ζ	–	test statistic for reverse arrangements test
μ	–	mean
μ_m	–	ratio of unsprung to sprung mass
σ	–	stress, true stress, standard deviation
σ'_f	–	fatigue strength coefficient
φ	–	AR coefficient
$\Phi(\hat{Z})$	–	CDF of normalised elevation values

Chapter 1: Introduction

A significant proportion of computer-aided engineering (CAE) applied to the field of automotive design depends on terrain topology to provide accurate excitations to multi-body and vehicle dynamics simulation packages. For example, when the suspension characteristics of a vehicle are to be evaluated and tuned, vehicle dynamics simulations require terrain profile data in order to simulate vehicle body motion as the tires move over bumps and potholes. While performing fatigue and durability simulations of chassis and suspension components, finite element models require input loads that are generally calculated using vehicle dynamics models of the vehicle's suspension, based on terrain profile data as the input excitation.

In order to simulate and predict vehicle body motion and component strength requirements accurately, it is important to possess accurate representations of the surface over which the vehicle will traverse in real world usage scenarios. Vehicle dynamics analyses require a representation of a vast number of different terrain types, in order to be considered statistically significant representations of realistic vehicle excitation. While it is possible to obtain physically measured topology of terrain, it is not feasible to obtain terrain data for every variety of terrain as this would involve working with extremely large datasets, which would be expensive to collect and maintain.

As virtual terrain is the basis on which all vehicle dynamics simulations are performed, accurate modelling of measured terrain would significantly reduce the gap in correlation between CAE simulations and physical test results. This work uses the methodology developed in previous research to generate synthetic terrain profile data by utilising mathematical models such as the autoregressive (AR) model and the Markov chain model to characterise measured terrain data that has been acquired by using a terrain measurement system. The measured and synthesised terrain data are analysed for

their statistical properties, in order to quantitatively compare the statistical conformity of the synthesised terrain to the measured terrain, as a means to assess the performance of the terrain models in capturing the statistical properties of the measured terrain. The synthesised terrain is then used as input excitation to a vehicle model in a multi-body dynamics application in order to obtain component loading histories for suspension control arms. Finite element analysis is then performed on suspension components in order to obtain fatigue life estimations of the component. Finally, some conclusions are made regarding the effectiveness of the terrain topology models in simulating the vehicle excitation content of the measured terrain.

1.1 Background

A terrain profile is defined as an indexed set of elevation values obtained at equally spaced longitudinal distances along the terrain being measured. These elevation values may be obtained by using a device known as a profilometer. Profilometers have been in use since the 1960s, and may range from simple contact-based handheld dipstick devices, to highly advanced vehicle-based non-contact elevation sensing devices such as the Vehicle Terrain Measurement System (Figure 1), an inertial profilometer.

Figure 1: Vehicle Terrain Measurement System

The VTMS is a 3-dimensional (3D) terrain surface measurement system developed in 2007 by the Vehicle Terrain Performance Laboratory (VTPL) at Virginia Tech. The terrain is scanned using lasers as the vehicle moves forward, and elevation values of the terrain surface are measured with millimetre accuracy [2, 3]. Using a Differential GPS (DGPS), an Inertial Measurement Unit (IMU) and a set of three co-planar accelerometers, the measured terrain elevation points are located in space and nominally corrected for vehicle body motion [3]. Thus, the terrain elevation points measured by the lasers are obtained as a point cloud, which can be rendered and visualised in terrain mapping applications, forming the 3D terrain surface. An example of rendered terrain data is shown in Figure 2 superimposed on a photograph of the actual surface.

Figure 2: 3-dimensional scan of terrain surface compared with the actual surface [4].

Terrain elevation points having uniform longitudinal spacing are then extracted using interpolation and gridding techniques described in [4, 5] and discussed in Appendix A to obtain a 2-dimensional (2D) terrain profile as shown in Figure 3. This terrain profile has been obtained from the Federal Highway Administration (FHWA), and

is part of its Long Term Pavement Performance (LTPP) program. The profile contains 6097 elevation points spaced 25 mm apart.

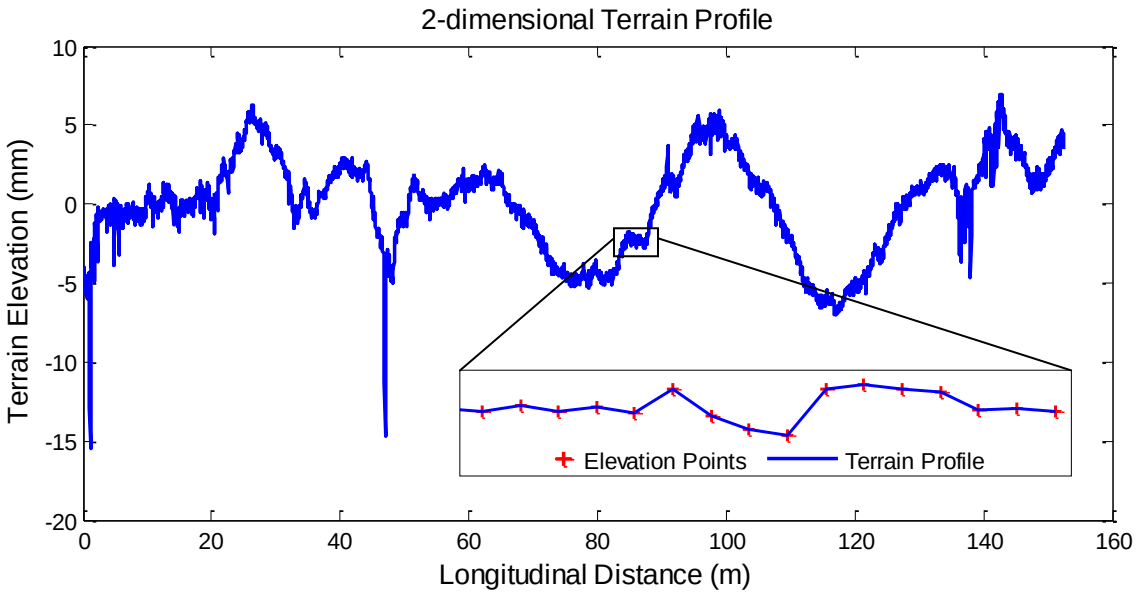

Figure 3: 2-dimensional terrain profile (inset: zoomed view of profile)

The work presented in this thesis is based on 2D terrain profile data obtained using the methods described above. Terrain profiles can be considered to be digital data signals, which may possess certain statistical properties such as Gaussianity (normal distribution), linearity, stationarity, etc. All the terrain modelling and statistical analysis procedures presented in this work are based on this premise. Moreover, these concepts of temporal signals are applied to the spatial terrain profiles used in this work. This implies that terrain profiles, which are spatial in nature, can be considered to be temporal in nature based on vehicle speed.

1.2 Objective

The objective of this work is to develop a methodology of robustly assessing the performance of terrain topology models in capturing the statistical properties as well as the vehicle excitation content of measured terrain profiles.

1.3 Approach

The work that has been done in order to achieve these objectives can be looked at in the following three stages:

1. Terrain modelling & synthesis
2. Statistical analysis of terrain
3. Vehicle modelling & finite element modelling

In the first stage, computer code was developed to parsimoniously represent measured terrain profiles as a set of coefficients in the case of the autoregressive model, and as a transition matrix in the case of the Markov chain model. This parsimonious representation is then used in order to generate synthetic terrain profiles of any length desired.

In the second stage, the synthesised profiles obtained in Stage 1 are analysed for their statistical properties in order to evaluate their statistical conformity to the measured profile on which they are based, and to obtain a quantitative measure of the same. For this purpose, the terrain profiles are considered to be discrete time-based signals and various statistical tests typical in time series analysis pertinent to terrain modelling are implemented for the analysis.

In the third stage, basic vehicle dynamics modelling using multi-body dynamics software is performed, wherein a virtual model of a vehicle is made to traverse the synthetic terrain generated in Stage 1. Vehicle component loading histories are obtained from this analysis, which are then applied to finite element models of the suspension components in order to obtain an estimate of the fatigue life of the components for that particular terrain. This procedure is also performed for the measured terrain, and a

comparison of the fatigue life calculated provides insight into the performance of the terrain models in capturing the vehicle excitation characteristics of the measured terrain.

1.4 Contributions

The two main technical contributions of this work are as follows:

- A Graphical User Interface (GUI) based software application has been developed which incorporates two terrain topology models, along with a methodology to evaluate the performance of these models in capturing the statistical properties of measured terrain profiles.
    - The autoregressive terrain model (developed by Wagner et al. [6]) has been implemented in order to characterise terrain of different types with a small set of coefficients.
    - The Markov chain terrain model (developed by Israel et al. [7]) has been implemented in order to characterise terrain of different types with sparse transition matrices.
    - Several statistical property tests have been implemented in order to analyse the properties of two-dimensional terrain profiles, and quantitatively evaluate the statistical agreement between measured and synthesised terrain profiles.

  This software application serves to integrate two main areas of research viz. terrain modelling and statistical analysis, in order to provide a single, all-inclusive resource for generating synthetic terrain profiles and evaluating their usefulness in modelling different types of terrain.
- The performance of the terrain models in capturing the vehicle excitation characteristics of the measured terrain has been evaluated through the estimation of suspension component durability on measured and synthesised terrain, by using vehicle kinematic models and finite element models of suspension components.

1.5 Organisation

This thesis is organised as follows:

- Chapter 2 presents a review of the state-of-the-art in terrain modelling and analysis.
- Chapter 3 summarises the theories underlying the methods applied in this work, and discusses the implementation of the theory. This chapter addresses each of the three stages of this work separately.
- Chapter 4 presents the results obtained from the application of terrain modelling and analysis methodology to several types of terrain. Additionally, the performance of these models in capturing vehicle excitation content, evaluated through finite element modelling, is presented.
- Chapter 5 summarises the work presented in this thesis along with discussions regarding its implication on virtual vehicle proving ground methodology. Potential areas for expansion of this work are also discussed.

This thesis is intended to include basic information and background to all the methods that have been applied in this work, in order to minimise the reader having to refer to other articles on the subject. However, emphasis has been laid on brevity, so as not to detract from the focus of the work.

Chapter 2: State-of-the-art

As stated previously, virtual terrain is the basis on which most vehicle dynamics simulations are performed. Hence, accurate modelling of measured terrain is required in order to enhance the simulation capability of ground vehicle performance. In this regard, many mathematical models have been applied to terrain data, in order to characterise terrain profiles and their properties.

Andren [8] provided a survey of the application of power spectral density (PSD) approximations to represent terrain profiles. The spectral range of the terrain profile is first decomposed into one or more bands, and a straight line approximation for the PSD is made for each spectral band. The equation of this line is then represented by the following formula:

$$G_d(n) = C\,\lambda^{-w} \qquad \text{(Equation 1)}$$

Here, G_d represents the roughness level of the elevation PSD, C is the unevenness index with units of m^3, λ is the wavelength with units of m, and w is a dimensionless parameter called waviness. It is to be noted however, that PSD of a signal presupposes the property of stationarity, which is violated by most terrain profiles. This limitation was overcome for example, by Rouillard, Bruscella, and Sek, who suggested a method for modelling terrain profiles based on their PSD [9-11]. Their methods focus on the underlying non-stationary and non-Gaussian nature of road profiles, and consider terrain profiles to consist of two fundamental components i.e. the steady-state terrain irregularities, and localised transient events. These transient events were identified and extracted through the use of statistical metrics, such as skewness, kurtosis and crest factor [12].

The steady-state irregularities in terrain profiles are subsequently shown to be stationary and Gaussian. Due to these properties, synthetic terrain profiles can be modelled on PSDs of the steady-state content of measured profiles. The transient events for the synthetic profiles are then generated with random amplitudes according to a Gaussian distribution, the mean and standard deviation of which are functions of the underlying RMS level of the measured profiles [11]. The probability density function (PDF) of the RMS level and the transient density of the measured terrain profiles are also characterised in order to classify measured terrain and generate synthetic terrain for simulation purposes.

Múčka and Kropáč [13] used hundreds of kilometres of U.S. highway terrain data from the Federal Highway Administration's (FHWA) Long Term Pavement Performance program (LTPP) to generate simulated terrain profiles consisting of 'obstacles' (i.e. bumps and potholes). The obstacles in the LTPP terrain data were identified and removed through median filtering. The probability density functions (PDFs) of the obstacle dimensions (i.e. length and height/depth, and distance between consecutive obstacles) were then obtained by fitting Weibull distribution functions to the extracted obstacles. For generating synthetic terrain profiles, obstacles were generated randomly using the PDFs obtained from the measured terrain, and superimposed on a randomly generated signal having a PSD defined by two parameters – the unevenness index C and the waviness w. This research resulted in the development of a tool called *obstaclegen*, for generating terrain profiles with randomly distributed obstacles.

Bogsjö and Forsén [14] generated synthetic terrain profiles by creating several stochastic spectral models of measured terrain profiles: the parametric road spectrum (PRS), shifted spatial range spectrum (SSR), direct spectrum estimation (DSE) and the transformed Gaussian distribution DSE (TrDSE). They also performed pseudo-fatigue assessment of the synthesised profiles to determine whether the models were able to capture the fatigue-inducing properties of the measured profiles, but it was found that the models were unsuccessful in that regard. As stated previously, spectral estimation of signals are only accurate when the signals are stationary.

In another publication, Bogsjö [15] proposed a method to assess irregularity in terrain profiles by studying the spectrogram of a high-pass filtered terrain profile. This spectrogram analysis allows frequency content of the terrain profile to be analysed in sections, and a Hanning window is used to scale the frequency input. In order to generate synthetic terrain profiles, a stationary Gaussian process is created, having spectral content similar to that previously analysed from the measured terrain profile, scaled by an exponent *a*. Two types of irregularities (short wavelength and long wavelength) are then added to this signal to simulate the rough parts of the terrain. The spectral densities of these irregularities are of the same form as the complete measured terrain spectrum, but restricted in frequencies and described by three parameters *b*, *c* and *w*. The parameters *a* and *w* are estimated from smooth sections of the terrain, while *b* and *c* are estimated from long- and short-wave irregularities. The synthetic profiles generated using this method were found to give pseudo-fatigue estimates that closer matched that obtained from the measured profiles.

Kern and Ferris [16] identified the autoregressive integrated moving average (ARIMA) model as one means to characterise road profiles by incorporating the uncertainty of terrain characteristics into the model. This uncertainty is captured in a residual process which may be represented by a single probability distribution function. The identification of the ARIMA parameters, the order of the AR model, the number of times the data were differenced, and the length of the moving average window was performed using the measured datasets.

The wavelet transform has been shown to be effective in describing localised roughness which is evident in terrain profiles and in comparing and classifying road profiles [17-19]. However, no attempt has been made to generate synthetic profiles using wavelet representation. Prah and Attoh-Okine [20] performed a comparative study of the Hilbert-Huang transform, the Fourier transform and the wavelet transform in pavement profile analysis, and showed that the Hilbert-Huang transform (HHT) preserves good spectral resolution in both distance and wave number domains. With this method, high-energy locations in the terrain profile can be more easily identified.

Apart from terrain synthesis, a lot of research has been done on analysis and classification of terrain profiles and their statistical properties. The most common methods of representing terrain characteristics are roughness indices. The most prevalent index for measuring terrain roughness is the International Roughness Index (IRI) [21, 22], which is defined as the suspension travel accumulation of a two-degree-of-freedom quarter car model, per unit length. This index is discussed in detail on page 21. The Ride Number [23] is a similar index, but the suspension travel accumulation is calculated with the root mean square (RMS) instead of absolute values. The Roughness Index for Driving Expenditure (RIDE) is designed to describe passenger discomfort potential by calculating the spectral density of sprung mass acceleration for a quarter car model traversing the terrain. Múčka and Kropáč [24] demonstrated that the IRI was insensitive to excitation of certain wavebands, and proposed an alternative metric to measure terrain unevenness [25], based on the unevenness index C and waviness w calculated from spectral density plots of the terrain. Moreover, the IRI was redefined in order to relate it to the parameters C and w.

Many researchers have also performed studies on the statistical properties of terrain profiles. Chaika and Gorsich explored the linearity and stationarity characteristics of terrain profiles and demonstrated that most terrain profile distributions are not Gaussian or stationary [26]. Other researchers have also explored the non-stationarity of terrain profiles [27-29]. Kern and Ferris demonstrated that significant correlation exists between successive measured data points on US highways [30]. Gorsich *et al* [31] compared road roughness metrics of different profiles. In [32], Bruscella *et al.* proposed a universal classification methodology for terrain profiles, by extracting the transient events from the measured profiles. Nine classification parameters were introduced in order to describe the spatial acceleration of the profiles (i.e. the double-derivative of the terrain elevation) based on the amplitudes of the transients, and RMS of the steady-state irregularities.

On reviewing all the literature on the subject of terrain modelling and analysis, it was noted that although there exist many methods of characterising measured terrain and synthesising terrain profiles, a reliable means of assessing the performance of each model

in capturing the vehicle excitation properties of measured terrain hasn't yet been implemented. Hence, the approach of this work has been to implement the autoregressive and the Markov chain models of terrain in order to generate terrain profiles, and assess their performance through the means of statistical analysis and finite element based fatigue analysis. The goal of this work is to provide researchers with a robust and non-partisan methodology to test the effectiveness of any terrain model in capturing the relevant properties of measured terrain faithfully.

Chapter 3: Theoretical Background & Methodology

This chapter provides an overview of the theoretical background to the work presented in this thesis. The author's contribution has been to integrate several areas of work in statistical analysis and mathematical modeling, and this chapter discusses the existing theoretical background that has been used in this work, and the manner in which it has been implemented. First, the concept behind the two terrain models i.e. the autoregressive model and the Markov chain model is explained, along with the reasons for choosing these models to represent terrain. Overviews of the implementation of these models are also discussed.

Next, the various statistical tests that have been implemented to analyse the statistical properties of terrain profiles are introduced and explained in detail. Reasons for choosing these particular properties for evaluating terrain are provided, with their implications on terrain characteristics. Further, *TerrainSim*, the GUI based application developed to enable users to analyse terrain and generate synthetic profiles, is introduced. Its features, capabilities and applications are then discussed. This is followed by a brief review of finite element method theory and application. An overview of the theory behind fatigue calculations is then provided along with a review of materials data required for this analysis.

3.1 Autoregressive Model

The autoregressive (AR) modelling technique is used to represent terrain profile data by assuming that the profile is a realisation of an underlying stochastic process. This technique was applied to terrain modelling by Ferris and Wagner [6]. In an AR model, the current value of a stochastic process (z_k) is represented as a linear combination of *l*

previous values in the process ($z_{k-1,}$ z_{k-2} ... z_{k-l}) scaled by a set of coefficients ($\varphi_{1,}$ φ_2 ... φ_l), and a residual process (a_k … a_N). This representation is shown graphically in Figure 4. The AR model is written as a difference equation in the following equation.

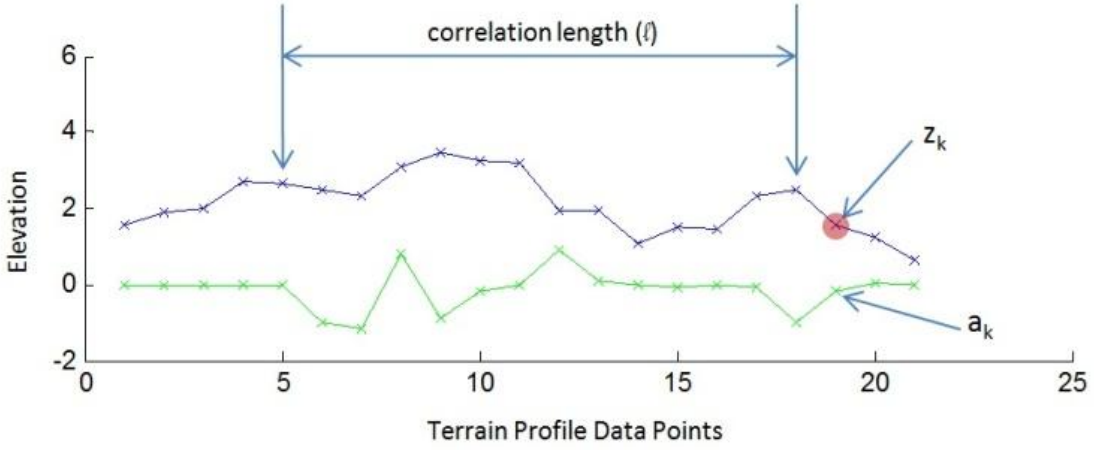

Figure 4: Characterising a terrain profile as an autoregressive model

$$z_k = [\, \varphi_1 z_{k-1} + \varphi_2 z_{k-2} + \ldots + \varphi_l z_{k-l} \,] + a_k \qquad \text{(Equation 2)}$$

The AR coefficients (φ_i) capture the linear behaviour of the series, while the residual process (a_k) captures the uncertainty. This model, when applied to a terrain profile, expresses the terrain height *z* at a point *k* as being dependent on the previous *l* points, subject to a scaling function φ. The issue with modelling terrain profiles with this technique is that they tend to vary according to a random walk process, producing a single pole near the unit circle. This is indicated by a prolonged correlation length of the partial autocorrelation function. However, the spatial derivative of the profile typically exhibits much shorter correlation lengths, so that the model order is determined for the *spatial derivative* of the profile and defined herein as *l*. Specifically, the order for the differenced data (*l*) is chosen at the lag at which the partial autocorrelation decays to within the 90% confidence limit. Since the spatial derivative of the original data is simply a first order difference equation, the model order for the original profile must be (*l+1*). Once the model order is determined, the parameterisation of the model must be

estimated. The initial estimate of the AR coefficients (φ_i) is derived via the Yule-Walker (autocorrelation) method based on the measured terrain profile. The issue of instability of the AR model is addressed in [6]. In order to maintain the stability of the AR model, the difference equation presented in Equation (1) is converted, using a z-transform, to a zero-pole representation and the AR model becomes an all-pole Infinite Impulse Response (IIR) filter. These poles must all have a magnitude less than unity, and if this is not produced by the Yule-Walker estimate of the coefficients, then it must be enforced. Once the coefficients have been determined and the model has been found (or forced) to be stable, the realisation of the residual process is calculated from the following equation.

$$\begin{bmatrix} a_k \\ a_{k+1} \\ \vdots \\ a_N \end{bmatrix} = \begin{bmatrix} z_k & z_{k-1} & \cdots & z_{k-l} \\ z_{k+1} & \ddots & & \vdots \\ \vdots & & \ddots & \vdots \\ z_N & \cdots & \cdots & z_{N-l} \end{bmatrix} \begin{bmatrix} 1 \\ -\varphi_1 \\ \vdots \\ -\varphi_l \end{bmatrix} \qquad \text{(Equation 3)}$$

This calculation produces a residual process having the same length as the measured profile. This residual process, however, is considered one realisation of an underlying stochastic process. In order to create a synthetic terrain profile, therefore, this process must be modelled. A statistical test by Wagner and Ferris [33] is used to determine if the residual process can be considered to be Independent and Identically Distributed (IID). However, no assumption is made, as is the standard practice, about the Gaussianity of the residual process. If the process is IID, then the process must be strictly stationary and the joint probability distribution is completely defined by a single Cumulative Probability Function (CPF). In this case, realisations of this residual process are simply synthesised by generating a uniform distribution of random numbers (between 0 and 1), equal in number to the length of the synthesised profile, and interpolating on the inverse CPF. The set of AR coefficients and residual process realisations thus calculated compose the set of model parameters that completely capture the physical characteristics of the terrain profile. This characterisation is then used to generate synthetic terrain. In order to initiate the process of generating synthetic profiles using the AR model described above, a set of random numbers are used (driving function).

3.2 Markov Chain Model

A first order Markov chain can be defined as a random process having the Markov property. For *discrete state* processes like a terrain profile, this means that the probability that the process assumes any particular value in the subsequent state depends only on the value of the current state in the process, and not on any preceding states. This property can be applied to terrain profiles, whereby the elevation value at a certain measurement point can be said to be dependent only on the value of the previous measurement point. Formally, this Markov property can be defined by the following relation:

$$P (Z_k = z_k \mid Z_{k-1} = z_{k-1}, Z_{k-2} = z_{k-2}, \ldots Z_1 = z_1) = P (Z_k = z_k \mid Z_{k-1} = z_{k-1}) \quad \text{(Equation 4)}$$

Here, Z_k denotes a family of random variables Z_k where k = 0,1,2…

z_k denotes the value of the random variable Z, where k = 0,1,2…

Stated another way, the Markov property states; 'conditioned on the present, the future is independent of the past'. The terrain profile shown in Figure 3 will be used as an example to demonstrate the representation of terrain profiles as a *finite-state, first order* Markov chain. In order to apply the Markov property to terrain profiles, the profile under consideration must first be discretised into a finite set of states. This set of states is called the state space of the Markov process. The first step is to decide the number of states into which the signal should be discretised. The upper bound of this number is limited by the resolution of measurement (z_{res}), while the lower bound is decided by desired accuracy. Before proceeding with the example, a few definitions must be introduced.

1. The set of states A must be *closed*. This means that once a random process acquires a value belonging to A, it can never acquire a value that does not belong to A.
2. The set of states A must be *irreducible*. This means that once a random process acquires a value belonging to A, it is possible to reach any state in A.

3. The *order* of a Markov chain is the number of preceding points that are said to influence any point in a process. For example, in a 2nd order Markov chain, the previous two points affect the value of the third point. This discussion is limited to first order Markov chains.
4. A *transition* is simply a change of state. A transition is said to occur from the first state i to the second state j. For a profile having 100 elevation points, the number of transitions is 99.

The highest possible number of states S_{max} that a terrain profile can be discretised into, can be calculated from the following formula:

$$S_{max} = round\left[\left|\frac{\max(z) - \min(z)}{z_{res}}\right|\right] + 1 \qquad \text{(Equation 5)}$$

For the terrain profile shown in Figure 3, the resolution is 0.1 mm, and the highest and lowest elevation values are 6.94 mm and – 15.5 mm respectively. Thus, for this profile, S_{max} = 225. However, for purposes of clarity in this example, a resolution of 1 mm will be used. Thus, the number of states S for a resolution of 1 mm will be 23. The terrain profile is then discretised into 23 states as shown in Figure 5. Here, the highest elevation value is assigned the 1st state, while the lowest elevation value is given the 23rd state. The possible advantages of irregularly spaced binning as it relates to estimating the transition probabilities is discussed in the Future Work section of this thesis. Note that the vertical axis has been inverted in order to preserve the orientation of the terrain profile. The next step in the process is to count the number of transitions that occurred from every state to all other states, in order to estimate the transition probabilities for the Markov chain. For this purpose, a transition matrix for the Markov model must be built. The transition matrix is a collection of transition vectors for each state i, where each transition vectors contains a count of how many transitions occurred from that state i to all other states j. The transition matrix can then be plotted as a 3-dimensional bar graph as shown in Figure 6.

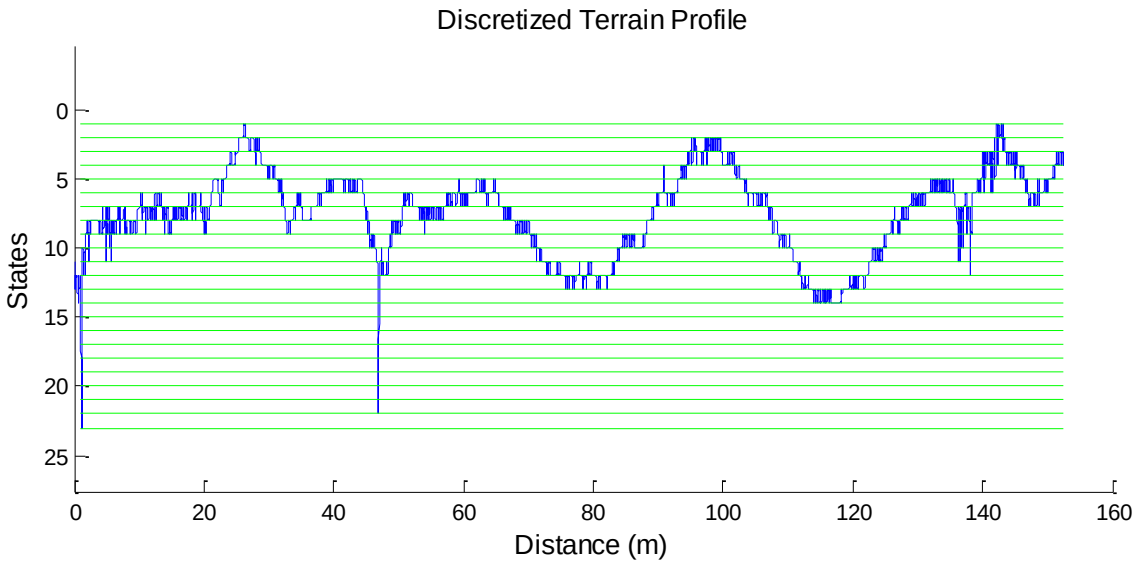

Figure 5: Discretised terrain profile

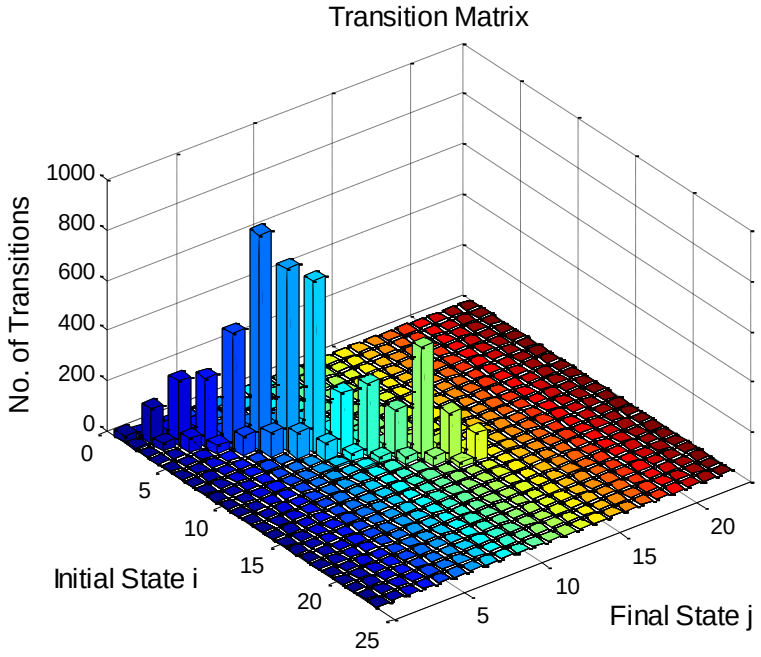

Figure 6: Transition Matrix

As an example, the state transition vector for the 6^{th} state is shown below. This is a vector which contains the count of transitions that occurred from the 5^{th} state to every other state in the state space (only the first 10 j states are shown). It can be seen that the most number of transitions took place from the 6^{th} state to the 6^{th} state itself. Further, most of the other transitions took place from the 6^{th} state to the 5^{th} or the 7^{th} state. This is expected, since the terrain profile under analysis is that of a U.S. highway where sudden large deviations are not common, and the binning is regularly spaced. Due to this property, it is seen that the entire transition matrix is leading diagonal-dominant, and is therefore a sparse matrix.

state j	1	2	3	4	5	6	7	8	9	10
no. of transitions	0	0	0	1	75	851	94	1	0	0

From the transition vectors, the transition probability vectors can be estimated, by dividing by the total number of transitions in the vector. This vector provides an estimate of the probability of reaching every state j, from a particular state i. For the above transition vector, the probability vector is as shown below. Clearly, the sum of this vector should be unity.

state j	1	2	3	4	5	6	7	8	9	10
transition probability	0	0	0	9e-04	0.07	0.83	0.09	9e-04	0	0

Next, the cumulative transition probability vector is calculated, which simply sums the probabilities for every state.

state j	1	2	3	4	5	6	7	8	9	10
cumulative probability	0	0	0	9e-04	0.07	0.90	0.90	1	1	1

A matrix of these cumulative transition probability vectors, for all states is then assembled, which fully characterises the measured profile as a set of probability vectors, which can be then used to continue the Markov process indefinitely. In essence, this is equivalent to extrapolating the measured terrain profile to a desired length, while introducing a stochastic character, at the same time maintaining its physical characteristics through the transition matrix. A new terrain profile can then be synthesised simply by starting the Markov process with a random number generated within the limits of the number of states (in this example, between 1 and 23). This will be the initial state i. The value of the subsequent state j will be obtained once again using a random number between 0 and 1, and matching that number to the cumulative transition probability vector for that state i. The probability function of the measured profile will be maintained through this method since the random numbers generated are uniformly distributed. Based on the above example, a synthesised profile generated using this method (with an increased resolution of 0.1mm) is shown in Figure 7.

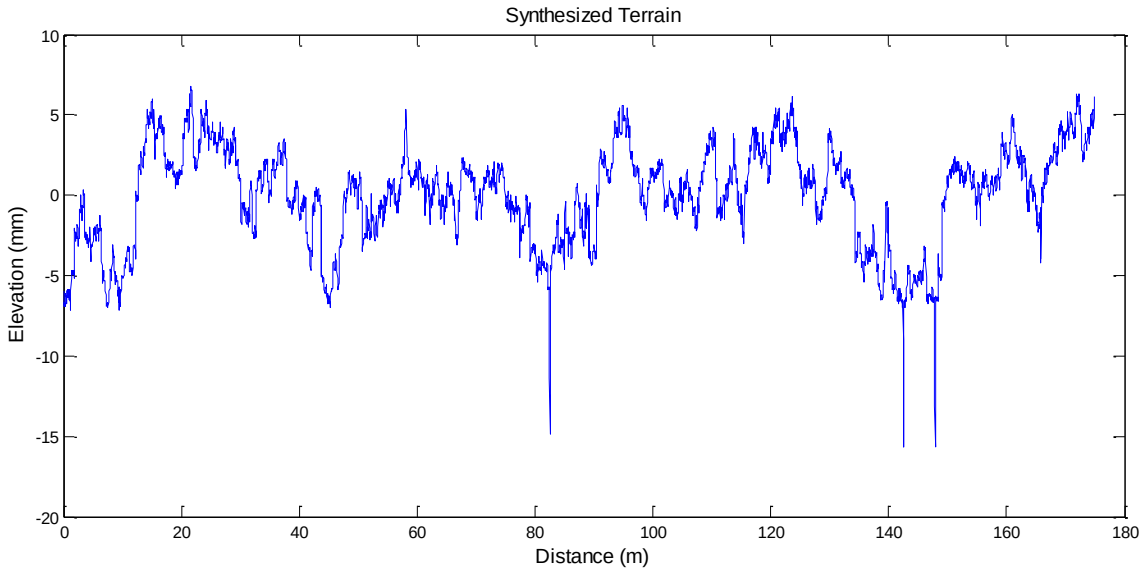

Figure 7: Synthesised terrain profile

3.3 Statistical Analysis of Terrain

Once the terrain profiles have been modelled and synthesised, it is important to ensure that the statistical properties present in the measured profiles are captured in the synthesised profile to a satisfactory degree. Certain statistical analyses provide some insight into the characteristics of the terrain which are pertinent to vehicle simulation. In this work, terrain profiles have been tested for the following statistical properties:

1. Gaussianity
2. Linearity
3. Stationarity
4. Time invariance
5. International roughness index
6. Rainflow count
7. Standard deviation

These properties were selected based on the state-of-the-art in terrain topology measurement and analysis, and are included here to provide a comprehensive statistical analysis of the terrain. The metrics obtained from each test are in the form of a cumulative distribution function (CDF), i.e. as a sorted distribution of the test statistic calculated for discrete segments in the terrain data. The same metrics are also calculated considering the entire terrain profile (instead of separate segments), yielding single metrics for the profile. This method of analysis provides information about terrain profiles at a local level as well as a global level, by analysing the profiles both as a whole, and in segments. Unlike previous work on terrain data analysis which focused on hypothesis testing, these statistical tests are not intended to find out *if* the data have a certain property, but to *what extent* that property exists in the terrain data.

For example, the results of the test for Gaussianity show how close the given data is to a Gaussian distribution. The main objective of obtaining a distribution of statistic metrics is to compare the strength of existence of every property at different locations

within the measured and synthesised terrain as a reliable means of comparing them statistically.

The terrain profile is evaluated in segments of length 15 m each, and each segment is considered a realisation of the same stochastic process. The statistic for each statistical test (apart from Gaussianity), is then calculated for all realisations. Thus, a vector of statistical metrics is obtained for each profile, by calculating the test statistic for the 15 m sections with no overlap, to reduce the dependence of sequential samples. For example, the first section evaluates the first 15 m of the profile, and the test metric obtained is assigned to this section. The next section is assigned the metric obtained by evaluating the section from the 15 m point to the 30 m point. This process is continued till the end of the profile is reached. In this manner, the roughest patches in the terrain profile can be identified easily, and a distribution of roughness values can be analysed to obtain better insight into the terrain sample's characteristics. The statistical tests implemented in this work are discussed briefly in this section.

3.3.1 Gaussianity

A Gaussian distribution of data is a distribution of values about a mean value (μ), having a variance of σ^2. A Gaussian distribution indicates that the data are clustered around the mean, the extent of which is indicated by the variance. Such distributions are also known as 'bell curves' since their probability distribution functions resemble the shape of a bell. It is common to assume that terrain profiles possess a Gaussian distribution. However, this assumption has been proved to be invalid in most cases, unless localised disturbances (e.g. bumps and potholes) are removed from the profile.

In this analysis, the distribution of the elevation values of the terrain profile is compared to a standard normal distribution in order to obtain a statistic of how closely the terrain data matches a normal distribution. The metric in this case is a measure of deviation of the sorted terrain values from the standard normal curve at each data point. The statistical test for Gaussianity is carried out as follows:

1. From the terrain data, the mean (μ) and variance (σ^2) are calculated.
2. The terrain data (z) are normalised by the mean and standard deviation as: $\hat{Z} = \frac{z-\mu}{\sigma}$ and then sorted in ascending order.
3. The cumulative distribution function (CDF) of the normalised data ($\hat{Z}$) is then calculated - $\Phi(\hat{Z})$.
4. The Empirical CDF of $\hat{Z}$ is calculated as: $ECDF(\hat{Z}_i) = \frac{n(i)}{N}$

   Here, *n(i)* is the number of $\hat{Z}$ values less than or equal to $\hat{Z}_i$, and N is the number of data points in the terrain profile. Since $\hat{Z}$ is ordered, the ECDF becomes a step function that increases by 1/N at each data point.
5. The test statistic D_N is then calculated as the supremum difference between the ECDF and the standard normal CDF of the terrain data, i.e.

$$D_N = \sup |ECDF(\hat{Z}) - \Phi(\hat{Z})| \quad \text{(Equation 6)}$$

The metric D_N represents the deviation of the terrain profile's elevation distribution from a standard normal or Gaussian distribution. This has been shown graphically in Figure 8 for a sample terrain profile. For hypothesis testing, the critical value of D_N (D_N^*) can be calculated using the procedures outlined in [34]. For large number of data, D_N^* can be estimated as:

$$D_N^* = \frac{C(\alpha)}{\sqrt{N}} \quad \text{(Equation 7)}$$

Where N is number of sample data

$C(\alpha)$ is a coefficient whose relation to the confidence level α is given as:

$$\alpha = 2 \sum_{i=1}^{\infty} (-1)^{i-1} e^{-2 i^2 C^2(\alpha)} \quad \text{(Equation 8)}$$

The plot of Gaussianity for the LTPP profile shown in Figure 3 has been shown in Figure 8. This plot shows the cumulative distribution function of $\hat{Z}$. The relation between α and C(α) according to the above equation is shown in Figure 9.

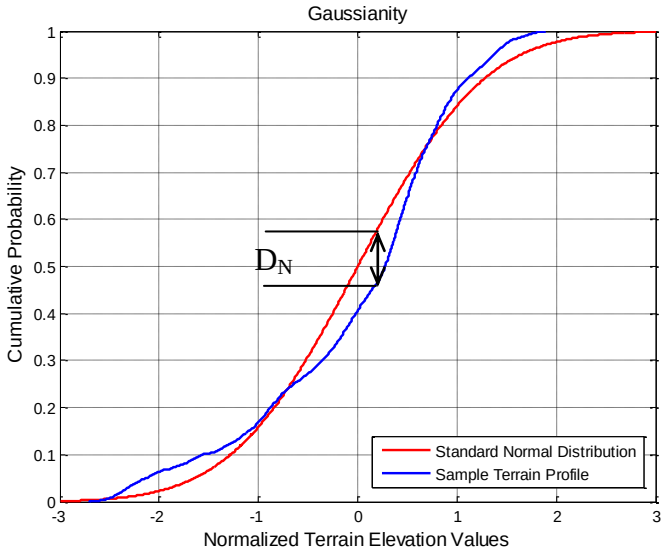

Figure 8: Plot of Gaussianity

For example, for a confidence limit of 95% (i.e. $\alpha = 0.05$) and a terrain profile containing about 7000 elevation points, $C(\alpha) = 1.36$ and $D_N^* = 0.01633$. If the value of D_N calculated for the terrain profile exceeds this number, the profile is said to have a non-Gaussian distribution.

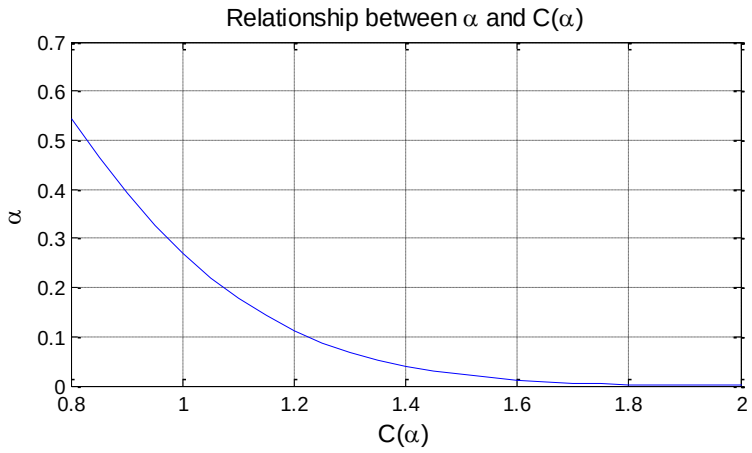

Figure 9: Relationship between α and C(α)

3.3.2 Linearity

Linearity of time-series data indicates that the data are linearly dependent on previous points without significant higher-order dependence (such as a dependence on the square or cube of the previous points). A procedure devised by Keenan [35] is used to test for linearity of the terrain profile data. Keenan's test statistic, *F*, is used as a metric of linearity by observing additivity in the profile. The procedure followed for this test is as described below.

Suppose X_1, X_2,... X_n is a stationary time series. It will be assumed that it is bilinear which means that it can be expressed as an expansion consisting of two parts. In symbols;

$$X_t = C + \sum_{i=-\infty}^{\infty} b_i \varepsilon_{t-i} + \sum_{i,j=-\infty}^{\infty} b_{ij} \varepsilon_{t-i} \varepsilon_{t-j} \qquad \text{(Equation 9)}$$

Here, ϵ_t is a random series (a series of random shocks), (b_i) and (b_{ij}) are each a sequence of constants and *C* is a constant. In this case, if X_t has a representation as a linear model, the constants b_{ij} in Equation (1) would be zero and consequently the data can be approximated by an autoregressive model of a sufficiently large order M, written AR(M). That is

$$X_t = a_0 + \sum_{j=1}^{M} a_j X_{j-t} + \varepsilon_t \qquad \text{(Equation 10)}$$

Here, a_j are constants and *M* is as described. The code for this test was developed to calculate the test statistic *F* for all realisations (i.e. F_1, F_2, ..., F_n), where the given profile is divided into segments of 15 m length each, and each segment is considered a realisation of the same stochastic process. The code is outlined as below.

Step 1 Regress X_t on ($1, X_{t-1}, \ldots, X_{t-M}$). M is a large but fixed integer. A value of 8 is used in this work, as suggested by Keenan [35], but can be changed. Calculate the predicted values called ($\hat{X}_t$) and let the estimated residuals be

called ($\hat{\varepsilon}_t$), for $t = M+1, M+2,\ldots, n$. Calculate the sum of the squares of the residuals: $\sum_t(\hat{\varepsilon}_t^2)$.

Step 2 To remove the effects of the correlation of ($1, X_{t-1}, \ldots, X_{t-M}$) on $\hat{X}_t^2$, regress $\hat{X}_t^2$ on ($1, X_{t-1}, \ldots, X_{t-M}$) and calculate the resulting residuals $\hat{\xi}_t$ for $t=M, M+1,\ldots,n$.

Step 3 Regress $\hat{\varepsilon}_t$ *on* $\hat{\xi}_t$ and calculate the regression coefficient $\hat{\eta}_0$.

Set $\hat{\eta} = \hat{\eta}_0\left(\sum_{t=M+1}^{n} \hat{\xi}_t^2\right)^{1/2}$.

Step 4 Calculate: $F = \frac{\hat{\eta}^2(n-2M-2)}{\sum_{t=M+1}^{n} \hat{\varepsilon}_t^2 - \hat{\eta}^2}$

Step 5 Repeat steps 1 to 3 for all n realisations and calculate $F_1, F_2, \ldots, F_n$

As explained previously, the test metric is calculated for 15 m sections, with no overlap. In this way, a distribution of local linearity of the measured and synthesised profiles is obtained, and can be compared by performing a two sample Kolmogorov-Smirnov test. The critical value of the F-statistic for the 95% confidence limit is 3.876 [36]. F-statistics above this value indicate non-linearity of the signal.

Linearity is a very useful property in time series analysis. It simplifies the representation of the series and makes it understandable and computable [37]. Figure 10 shows two sections of the LTPP profile having different values of Keenan's statistic F. The section on the right was classified as being linear, while the section on the left was classified as nonlinear. Figure 11 shows the cumulative distribution function for the *F-statistic* for the LTPP profile. This plot can be used effectively to compare the distribution of test statistics for two or more profiles.

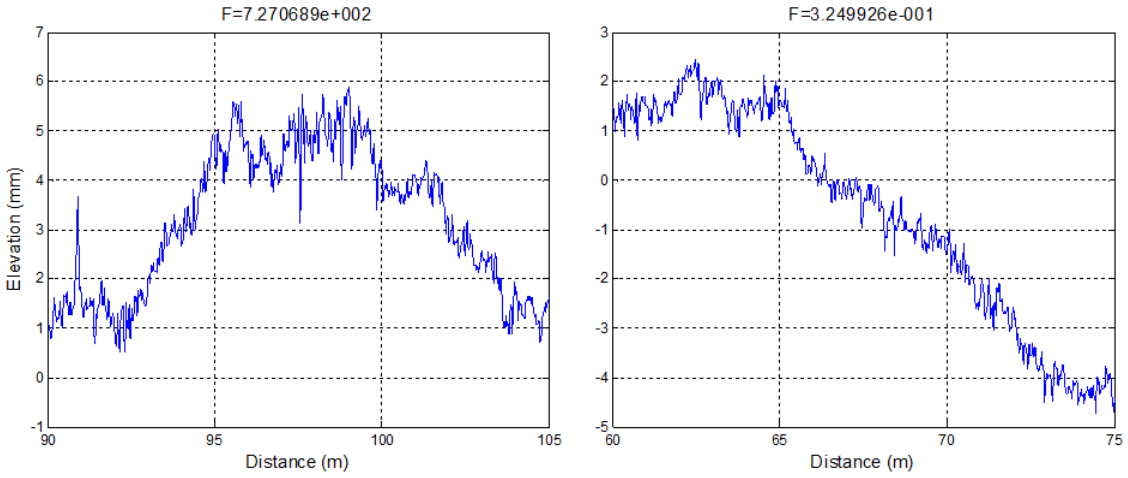

Figure 10: Comparison of linear and non-linear sections of the LTPP profile

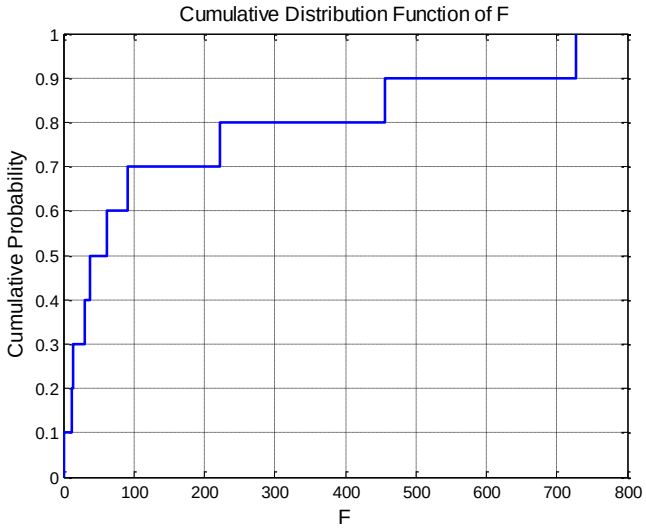

Figure 11: Cumulative distribution function of *F-statistic* for the LTPP profile

3.3.3 Stationarity

A random process is considered to be stationary (in a wide sense), when both its mean value (first moment) and auto-correlation function (joint moment) are time-invariant [38]. Stationarity of a process indicates there is no significant trend in the signal, and that its statistical and spectral properties are time invariant. Note that stationarity is a temporal property, but will be applied to the terrain profile data

interchangeably with homogeneity, which is an equivalent spatial property. Stationarity of a terrain profile is a very useful property, and allows the use of statistical techniques such as spectral analysis.

As a measure of stationarity, a *reverse arrangements* test is performed on the terrain profile. In this simple test, each data point in the time series is considered individually. The value of that data point is then compared with all other points that follow it, and the number of times that its value exceeds the following points is calculated. This is said to be the number of *reverse arrangements* in the data. A test statistic (ζ) is then calculated according to the following formula [39]:

$$\zeta = \frac{A - \left[\frac{N(N-1)}{4}\right]}{\sqrt{\frac{2N^3 + 3N^2 - 5N}{72}}} \qquad \text{(Equation 11)}$$

Here, *A* is the total number of *reverse arrangements* in the profile, and *N* is the total number of data points in the terrain profile. Since this test provides one test statistic (ζ) per profile, the profile is evaluated in segments of 15 m, as described previously. A vector of ζ values for each profile is then obtained. A signal is said to be stationary with 95% confidence if $|\zeta| < 1.96$ [39]. The assumption of the existence of a PSD presupposes stationarity [40], hence the evaluation of this property provides insight into whether the spectral content of a terrain profile should be evaluated in individual sections if it is non-stationary, or as a whole in case it is stationary. Figure 12 shows two sections of the LTPP profile. The section shown on the left, as indicated by its test statistic value, is considered slightly nonstationary, and the section on the right was seen to be highly nonstationary. Chaika et al [37] made the following conclusions regarding stationarity in terrain profiles:

1. Long sections of terrain profiles are not stationary.
2. Short sections of terrain profiles may not be stationary depending on their content and characteristics.

3. Generally smooth roads are stationary, but rough roads are not.

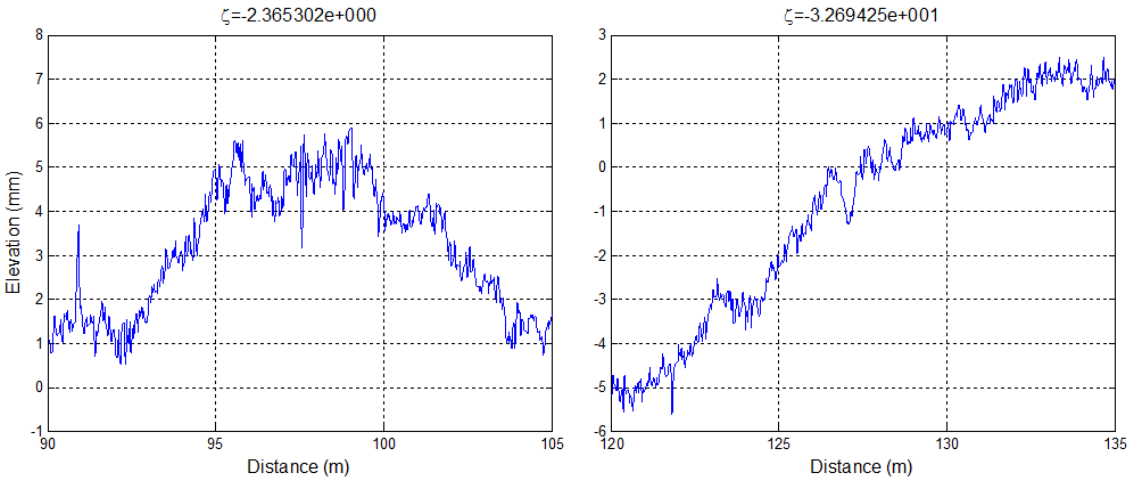

Figure 12: Comparison of stationary and non-stationary sections of the LTPP profile

3.3.4 Time invariance

The time invariance of a signal can be evaluated by the method described in this section. The data points in the signal are evaluated in 15 m sections as described previously. The value of the time average of the entire signal is then compared to all points in a group, and the probability p_{ti} is calculated, of the value of the time average being greater than the value of a data point in that group. This is done by ordering the data points in the group, and identifying what percentage (fraction) of values is smaller than the time average.

$$p_{ti} = \frac{\sum_{i=1}^{N_g} \frac{1 + sgn\,(z_{avg} - z_i)}{2}}{N_g} \qquad \text{(Equation 12)}$$

Here, z_{avg} is the time average of the group, and N_g is the number of points in the group. A vector of p_{ti} values is thus obtained, one for each group in the profile. For a perfectly time invariant signal considered as a single section, 0.5 would be computed for the test statistic since the probability of the time average of the signal being greater than any data point value will be 0.5 (i.e. 50% probability). This is because for a time invariant signal, approximately half the data values exceed the time average value of the

signal. However, this is a necessary, but not sufficient condition for time invariance, and Type II errors are common with this test. Figure 13 shows the distribution of p_{ti} throughout the LTPP profile. The area between the curve and the line drawn at $p_{ti} = 0.5$ provides an indication of time invariance. Since a more time invariant signal would yield metric values close to the expected value of 0.5, the area between the two curves would be inversely proportional to the time invariance property, with low values of area indicating high time invariance properties. A perfectly time invariant signal (under certain conditions) would yield metric values equal to 0.5 in all sections, yielding no area between the curves.

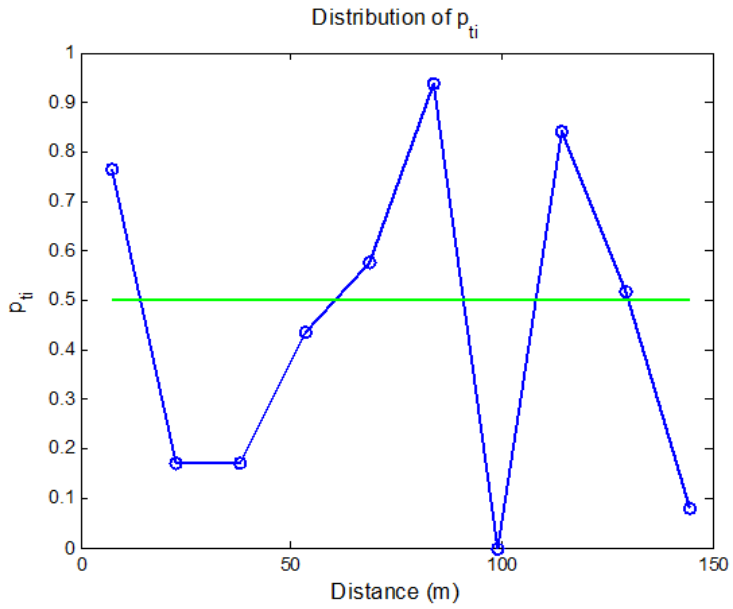

Figure 13: Distribution of time invariance throughout a terrain profile

3.3.5 International Roughness Index

The International Roughness Index (IRI) is a metric that describes pavement roughness in terms of the suspension accumulation of a two degree of freedom quarter car model, i.e. the number of inches per mile (or m/km etc.) that the suspension travels, as the model traverses the terrain profile. The lower the IRI number, the smoother the ride is said to be. The IRI has been shown to be effective in providing a consistent indicator of pavement condition, especially the roughness qualities that affect vehicle response. In the calculation of the IRI for a road surface, two filters are used:

1. 250 mm moving average filter: to simulate the enveloping behaviour of pneumatic tires and to reduce the sensitivity of the IRI calculation to the data interval [22].

2. Quarter car filter: to simulate the dynamic effects that determine how road roughness causes vibrations in a vehicle [22].

The National Cooperative Highway Research Program (NCHRP) developed the 'Golden Car' – a set of parameters that best represent average vehicle parameters. These set of parameters are used in the IRI calculations, and are as follows:

a. $c = c_s/m_s = 6.0$

b. $k_1 = k_t/m_s = 653$

c. $k_2 = k_s/m_s = 63.3$

d. $\mu_m = m_u/m_s = 0.15$

In these parameters, m_s is the sprung mass, m_u is the unsprung mass, c_s is the damping coefficient, k_t is the stiffness of the tire, and k_s is the stiffness of the spring, and μ_m - ratio of unsprung to sprung mass. A vehicle velocity of 80 km/h is assumed while calculating the IRI. The IRI is calculated as:

$$IRI = \frac{1}{L}\int_0^{L/V} |\, \dot{z}_s - \dot{z}_u \,|\; dt \qquad \text{(Equation 13)}$$

In this equation, $\dot{z_s}$ is the vertical velocity of sprung mass, $\dot{z_u}$ is the vertical velocity of unsprung mass, L is the length of the terrain profile, and V is the forward velocity of the vehicle. The vertical velocities of the sprung and unsprung masses are calculated by approximating the vehicle as a 2 degree-of-freedom spring-mass system. A representation of this spring-mass system is shown in Figure 14.

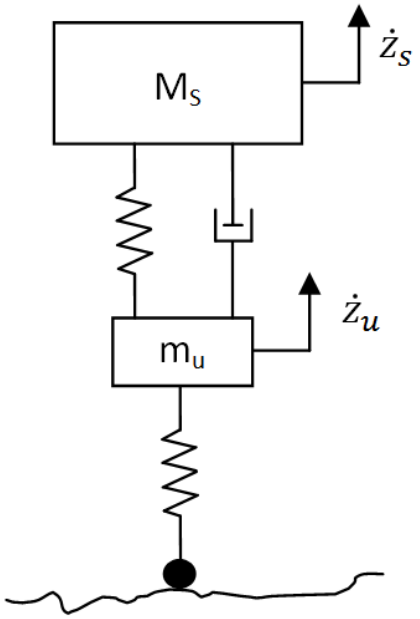

Figure 14: 2 degree-of-freedom quarter car model

Full details regarding the algorithm for calculating IRI can be found in [22], and the complete equations have been included in Appendix B. Apart from calculating the IRI of the entire terrain profile, the IRI is calculated for 15 m long sections of the profile with no overlap, in order to obtain a set of local IRI values throughout the profile. Typical IRI value ranges of different type of pavements are shown in Figure 15. Figure 16 shows the sections of the LTPP profile having the highest value of IRI (right) and the lowest value of IRI (left). It can be seen that the section on the right has higher amplitude disturbance events as compared to the section on the left, as well as a single high magnitude feature, leading to higher values of IRI.

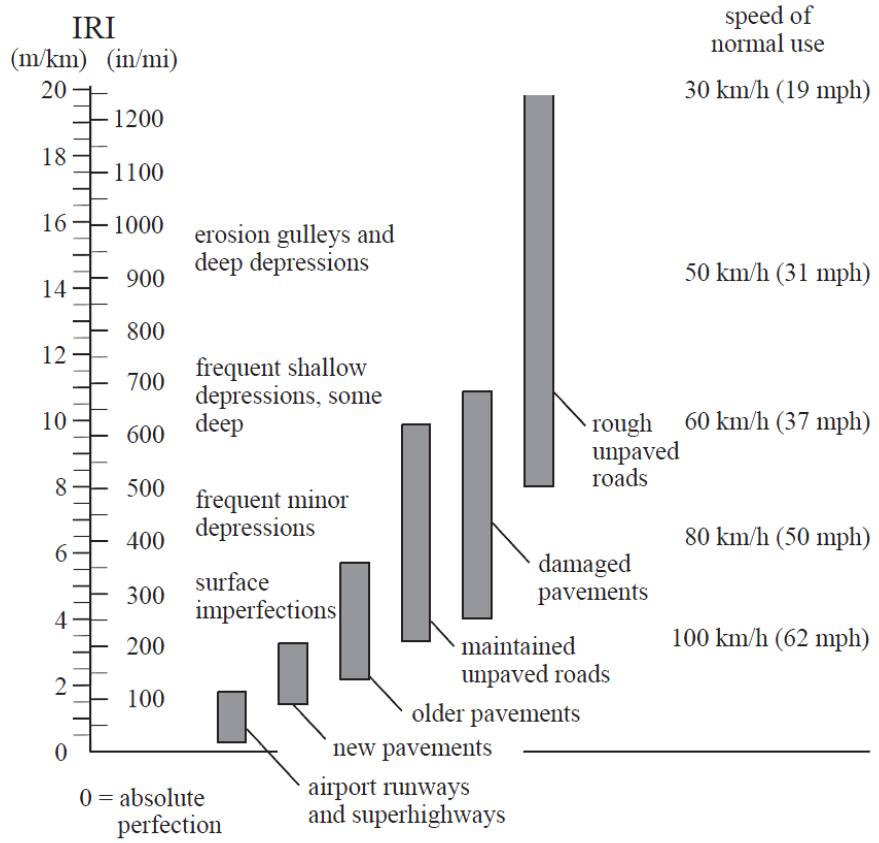

Figure 15: IRI value ranges for different types of pavements [1]

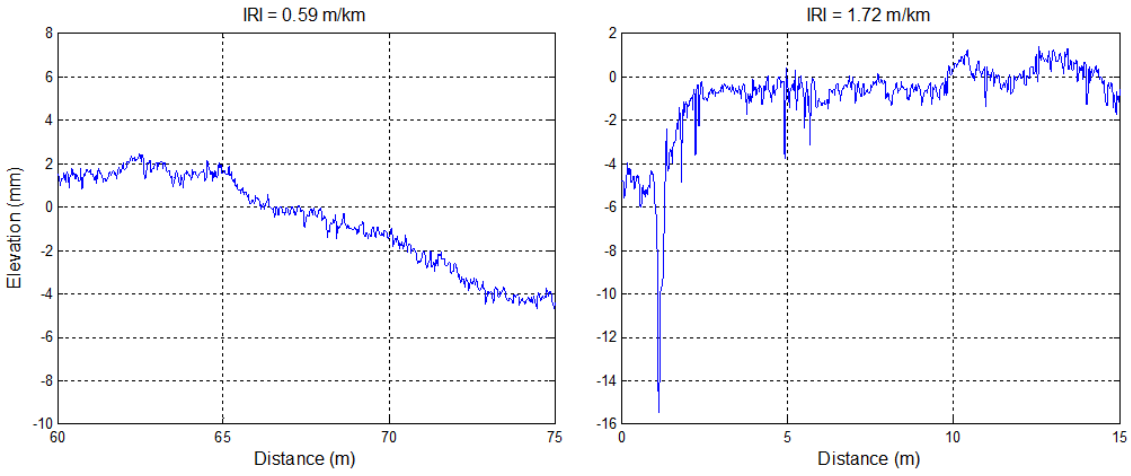

Figure 16: Comparison of smooth and rough sections of LTPP profile

3.3.6 Rainflow count

Rainflow counting is a method of identifying complete cycles (closed hysteresis loops) in a time history. It was originally intended to simplify the testing of the stress-strain response of a material subjected to random loading into a set of simple stress reversals, but can also be applied for various other purposes, including the statistical analysis of terrain profiles. The number, amplitude, and mean of reversals in a terrain profile indicate roughness, the scale of which may vary. There are several methods available for counting rainflow cycles. The algorithm developed by Niesłony [41] based on the ASTM standard [42] of rainflow counting has been used in this work. This method allows the identification of half and full rainflow cycles along with their mean values and amplitudes. Rainflow counting is being increasingly accepted in the terrain profiling community as a reliable means of expressing the roughness of a terrain profile. The ASTM standard rainflow counting algorithm can be summarised as follows:

1. Starting from the first point, three points are considered, x, y and z. The elevation ranges between x and y and between y and z are named X and Y respectively.
2. If $|X| \geq |Y|$, one cycle is counted, and the points y and z are discarded. The elevation range for the cycle is the value of Y.
3. This process is completed till the end of the profile is reached.
4. The same steps are then applied to all the remaining points. This process is continued till all points are discarded.

The rainflow count is performed for 15 m long sections with no overlap, as well as for the entire profile. This statistic is useful in terrain analysis since it provides a count of reversals in elevation values in the terrain profile, which directly affects the ride of a vehicle traversing that terrain. Figure 17 shows the sections of the LTPP profile having highest and lowest rainflow count. The section on the left has a higher number of reversals, although the section on the right has higher amplitude events.

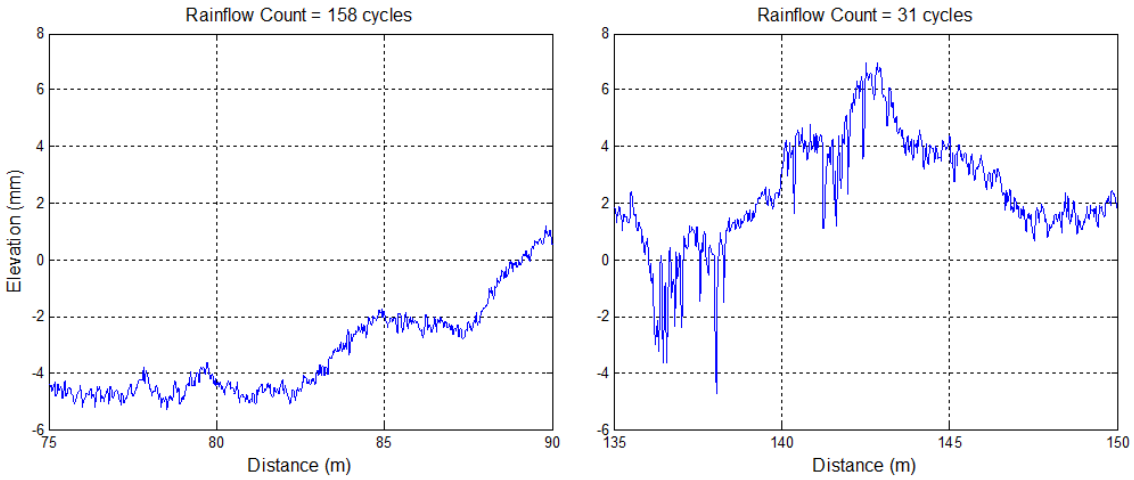

Figure 17: Sections of the LTPP profile having highest and lowest rainflow count

In a similar manner, the RMS, mean, median and standard deviation of the 15 m long sections are also calculated and CDFs of their distributions are obtained. The comparison of these CDFs in order to obtain a quantitative measure of statistical similarity between two terrain profiles is discussed in the next section.

3.4 Statistical Comparison of Terrain

As mentioned previously, every statistical property metric is obtained as a distribution of metric values for discrete sections throughout the profile. The distribution of each of these metrics for two different profiles can then be compared using a two-sample Kolmogorov-Smirnov test as implemented in MATLAB. This test is a statistical procedure to check the level of agreement between two sample distributions. This is done by plotting the two curves simultaneously, and calculating the absolute value of deviation between them. The probability of the two sets of metrics originating from similar processes is then calculated by using the formula shown below. This value is dependent on the absolute value of deviation between the two distributions D_n, and the number of samples in the distributions n_1 and n_2.

$$p = e^{-2\left(\left(\sqrt{\frac{n_1 * n_2}{n_1 + n_2}} + 0.12 + 0.11\sqrt{\frac{n_1 + n_2}{n_1 * n_2}}\right) D_n\right)^2} \qquad \text{(Equation 14)}$$

This is equivalent to the probability that the two distributions are realisations of the same underlying stochastic process, and are therefore statistically similar. For example, a *p-value* of 1 for IRI indicates that the two profiles have identical distribution of roughness throughout their length. Figure 18 shows a representation of how the Kolmogorov-Smirnov test compares two distribution curves. The confidence bounds are calculated based on the level of significance selected, and the null hypothesis (that the two distributions are statistically similar) is rejected if the maximum value of deviation between the two curves exceeds the limits of the confidence bounds.

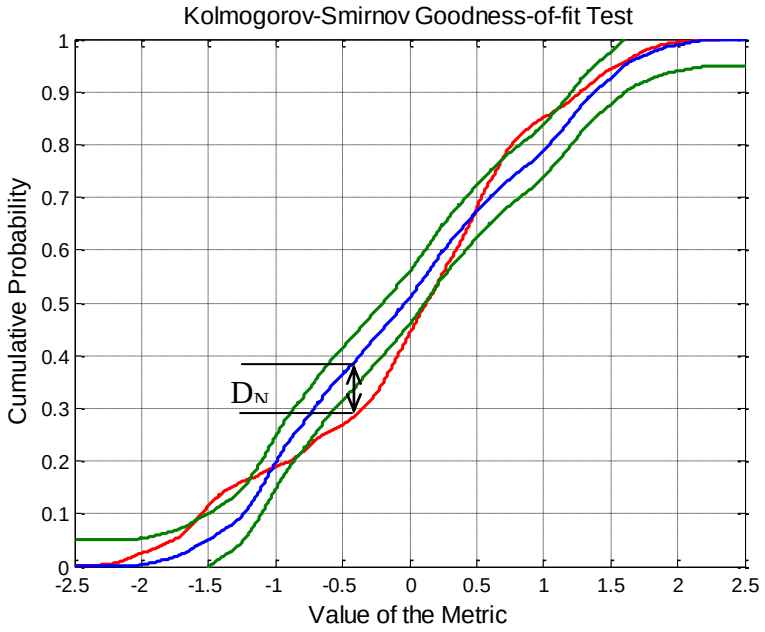

Figure 18: Comparing two distributions using the Kolmogorov-Smirnov test

This comparison is done for the distribution curves of every statistical metric, resulting in a series of *p-values*. A weighted average of these *p-values* is then calculated to obtain a quantitative measure of overall statistical similarity, called the *G-value*. The weighting for each of the properties can be chosen based on the application of comparison. For example, if the IRI is considered more important while comparing two profiles for vehicle ride analysis, it is given more weight compared to the other statistics. For surface texture studies, the rainflow count statistic may be considered more important. Further investigation into the statistical properties of typical terrain types will reveal more information regarding which property is important for which application.

3.5 *TerrainSim* – Terrain Modelling Software

As part of the work that has been done on terrain modelling and analysis methodology, a MATLAB based software application called *TerrainSim* has been developed. *TerrainSim* is intended to allow researchers to generate synthetic terrain profile data by using the autoregressive model and the Markov chain model to capture the physical characteristics of measured terrain data. Additionally, *TerrainSim* contains various statistical analysis tools discussed previously, to enable researchers to gain insight into the characteristics of the terrain locally as well as globally. The graphical user interface (GUI) of *TerrainSim* provides an intuitive means to do so. The analysis techniques also provide a means to obtain a quantitative comparison of the performance of the terrain model in modelling measured terrain.

The Graphical User Interface (GUI) for *TerrainSim* has been developed with the intent of allowing the user to quickly select input files, plot the desired outputs and compare results by varying parameters. The ability to compare measured and synthesised profiles at the desired level of magnification provides good visualisation of the modelled terrain profile. The user is also able to select different output formats for direct input to vehicle dynamics software and save data plots for further analysis. A screenshot of the GUI is shown in Figure 19.

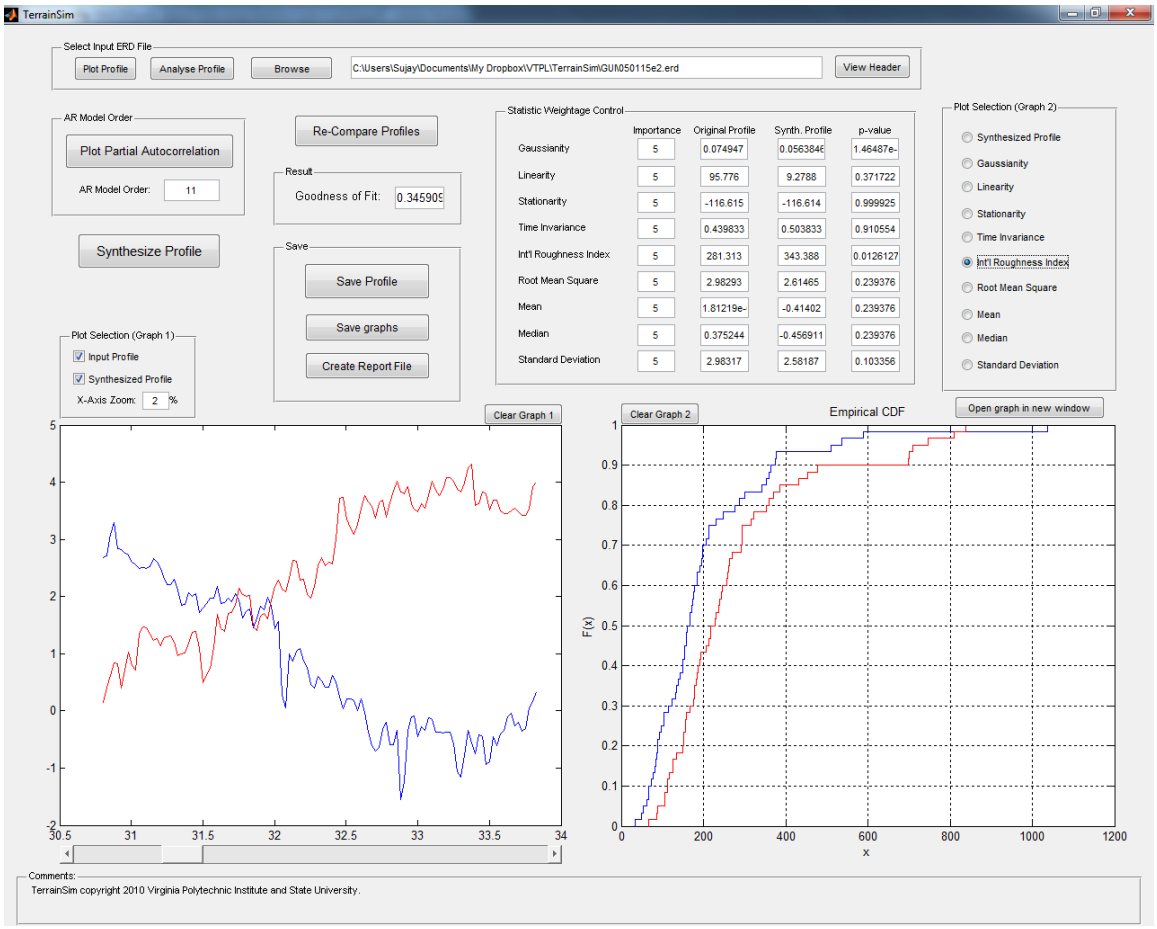

Figure 19: *TerrainSim* user interface

3.6 Finite Element Modelling & Fatigue Analysis

The final aim of this work is to study the performance of terrain models in capturing the excitation characteristics of measured terrain of different types with respect to the effect of the terrain on the reliability of suspension components. The best way to do this is to simulate a virtual vehicle traversing the synthesised terrain as well as the measured terrain and obtain loading histories for critical suspension components using vehicle dynamics analysis. Next, the stress and strain distribution on the components is calculated through finite element modelling of the suspension components. Finally, theories of fatigue failure are applied to calculate the service life of the components.

In this work, the main focus has been terrain modelling and analysis, and finite element analysis has been used as a tool to assess the performance of the terrain models. This has been done using commercial software applications, and as such, the theory behind these methods has not been studied. However, basic understanding of the principles behind these methods is important, and has been treated at a basic level in this section.

Finite element analysis is an efficient method of solving for a spatial distribution field within a structure which is to be analysed. The field to be calculated could be displacement, temperature etc. This work deals with displacement, stresses and strains, and therefore the FE method has been applied to calculate the displacement field within the suspension components under analysis.

The structure is first discretised into a *finite* number of *elements*, called a mesh of elements. The number of elements used depends on the size and complexity of the component, accuracy required, and computation time allowance. The category of element used (1D, 2D or 3D), as well the type (e.g. triangular, quadrilateral, tetrahedral, hexahedral etc.) depends on the geometry of the structure and the nature of the problem. In this work, two suspension components of the Volkswagen Jetta (Mark V) have been modelled using the finite element method. The front lower control arm (LCA), which is a forged aluminium component, has been modelled using 3D tetrahedral elements, while

the rear LCA, which is a sheet metal component has been modelled using 2D quadrilateral and triangular elements.

Figure 20: Tetrahedral mesh of Jetta front lower control arm

Figure 21: 2D mesh of Jetta rear lower control arm

The displacements at the vertices of each of these elements (called nodes) are calculated using the formula:

$$[K]\{u\} = \{F\} \qquad \text{(Equation 15)}$$

Here, *K* is the stiffness matrix which is dependent on the material properties as well as the structure of the component. It can be obtained using a number of different methods, the most popular being the Galerkin method. *u* is the vector of displacements along each direction, at each of the nodes, and *F* is the vector of external forces applied along each direction, at each node. In the suspension components that have been modelled here, forces are only applied at mounting locations at the chassis and the wheel carrier. These forces are applied uniformly at all the nodes which lie within the mounting location (i.e. around the bushing or bolt location).

The displacements within each element are then calculated from the displacement at the nodes of that element, using simple interpolation techniques (usually linear or quadratic). For example, the displacement field within a quadrilateral element can be calculated from its four vertices (*a*, *b*, *c* and *d*), using the formula

$$u_x = N_a u_{xa} + N_b u_{xb} + N_c u_{xc} + N_d u_{xd} \qquad \text{(Equation 16)}$$

Here, u_x is the displacement along the x-axis at a distance *x* from node *a*, while *N* is a shape function which may be linear or quadratic in *x*. This interpolation of displacements within an element is only an approximation using the displacements calculated at the nodes, and hence the accuracy of calculation is increased with smaller elements (i.e. a finer mesh). However, this is at the cost of increased computation time.

From the calculation of displacements, strain can be calculated using one of several formulations. For example, Cauchy's simplified strain formulation relates strain as the partial differential of displacement with respect to each directional vector. The stress distribution can then be computed using the stress-strain relation which is given by:

$$\{\sigma\} = [C]\{\varepsilon\} \qquad \text{(Equation 17)}$$

Here, σ is the stress ε is the strain. *C* is a characteristic matrix which depends on the properties of the material. The procedure outlined above is applicable for linear elastic analysis, in which the load-displacement or stress-strain curves are linear (i.e. a straight line). In such cases, the stiffness matrix *K*, and the characteristic matrix *C*

contain constant values. However, this is an idealised situation, considering that the material experiences only elastic (completely reversible) deformation. In reality, the material properties vary with increasing stress and strain. Detailed material property information is required in order to formulate stiffness and characteristic matrices that vary with stress and strain. The FE modelling in this work has been performed with the assumption of a Hookean material (i.e. the material follows Hooke's law for all stress and strain levels).

As the vehicle model traverses the virtual terrain, forces exerted on the suspension components keep varying. Thus, a 'loading history' is obtained for each force location. This loading history is applied to the FE model, in order to obtain a stress and strain history corresponding to incremental steps in time. When there are several loads acting on a component, each having independent histories, the principle of linear superposition is used to combine the loads together to determine the stress variation at each node. The equation for linear superposition is as follows:

$$\sigma_{ij}(t) = \sum_{k=1}^{n} \frac{\sigma_{ij,k}}{P_{FEA,k}} P_k(t) \qquad \text{(Equation 18)}$$

Here, n is the number of different loads, $P_k(t)$ and $\sigma_{ij}(t)$ are the time-varying load history and stress tensor respectively, and $P_{FEA,k}$ and $\sigma_{ij,k}$ are the load magnitude and stress tensor for the k^{th} load, obtained from FE analysis.

The fully elastic stresses and strains that were calculated using linear elastic FEA can then be converted to the equivalent non-linear elastic-plastic stresses and strains that occur in high stress regions like notches, by using Neuber's correction. For limited yielding (perfectly plastic deformation), Neuber's rule states that:

$$\sigma\, \varepsilon = K_t^2\, (Se) \qquad \text{(Equation 19)}$$

$$K_t = \sqrt{K_\sigma\, K_\varepsilon};\quad K_\sigma = \frac{\sigma}{S};\quad K_\varepsilon = \frac{\varepsilon}{S} \qquad \text{(Equation 20)}$$

Here, σ and ε are the local (plastic) stress and strain, and S and e are the nominal (elastic) stress and strain. K_t is the theoretical stress concentration factor, K_σ is the true stress concentration factor, and K_ε is the true strain concentration factor.

The stress and strain histories calculated represent a variable amplitude, random loading sequence. However, fatigue properties of materials can be obtained only for fully reversed, constant amplitude cycles in the form of stress-life or strain-life curves. In order to relate the variable amplitude, random loading sequence to the material data, they are reduced to equivalent constant amplitude cycles using the method of cycle counting. Cycle counting is the method used to count the number of stress-strain hysteresis loops and keep track of their range and mean values. The most popular method of cycle counting is the rainflow method, which has been dealt with in 3.3.6. Thus, the random variable amplitude loading sequence can be reduced to a series of equivalent completely reversed cycles occurring at different stress levels, to which the traditional theories of fatigue failure can be applied.

Two main theories of fatigue failure can now be considered; the stress-life (S-N) theory and the strain-life (ε-N) theory. The S-N theory relates component life to stress, assuming a linear relation between stress and strain (i.e. assumes all strain to be elastic). It is based on the Wöhler diagram which is a plot of cycles to failure of a test specimen subjected to alternating bending stress. This theory is reasonably accurate for high-cycle fatigue (i.e. life of > approx. 10^5 cycles). For low cycle fatigue (i.e. life of < approx. 10^5 cycles), plastic strains are prevalent and the stress-strain relation is non-linear. In random loading histories such as those typically found in suspension excitation, plastic strains are prevalent, which significantly affect fatigue life predictions. Hence in this study, the ε-N theory is used, which relates component life to strain by the following relation:

$$\varepsilon_t = \varepsilon_e + \varepsilon_p \qquad \text{(Equation 21)}$$

$$\varepsilon_t = \frac{\sigma_f' \left(2N_f\right)^b}{E} + \varepsilon_f' \left(2N_f\right)^c \qquad \text{(Equation 22)}$$

Here, ε_t is the total strain and ε_e and ε_p are the elastic and plastic strains. σ_f' is the fatigue strength coefficient and ε_f' is the fatigue ductility coefficient, while *b* and *c* are the fatigue strength and fatigue ductility exponents. These are properties of the material that can be obtained from the testing of a specimen subjected to completely reversed loading (i.e. the ε-N curve). $2N_f$ is the number of cycles to failure. This relation was later modified by several researchers to account for the effects of residual mean stresses. The Smith-Watson-Topper modified strain-life relation is as follows:

$$\sigma_{max}\,\varepsilon_t = \frac{(\sigma_f')^2\,(2N_f)^{2b}}{E} + \sigma_f'\,\varepsilon_f'(2N_f)^{b+c} \qquad \text{(Equation 23)}$$

The theories and methodology that have been discussed above now come together in the form of Palmgren-Miner's linear damage summation rule, which states that the total damage that is inflicted on a component subjected to a random loading history, is a linear sum of damage caused by all of the equivalent fully reversed sequences:

$$\sum_{i=1}^{l} D_i = \sum_{i=1}^{l} \frac{n_i}{N_i} \qquad \text{(Equation 24)}$$

Here, D_i is the damage caused by a sequence of equivalent reversed loading at a particular stress level. The total damage caused is then the sum of damage caused by all sequences of reversed loading. N_i is the reversals to failure at a particular stress level, and n_i is the number of reversals at that stress level that exist in the loading history. The component is said to have failed due to fatigue if $\sum D_i \geq 1$. The linear damage summation theory is applicable to both S-N and ε-N theories of failure. The total fatigue life is simply the reciprocal of the total damage calculated from Miner's rule.

The finite element models of the Jetta suspension components have been formulated using the inertia relief method of FEA used for analysis of free structures. This method of analysis is based on d'Alembert's principle of inertial forces, which states that 'the sum of applied forces and inertial forces for a dynamic system does no virtual work'. In equation form, d'Alembert's principle can be stated as:

$$\delta W = \sum (F_i - m_i a_i)\, \delta r_i = 0 \qquad \text{(Equation 25)}$$

Here, δW is the virtual work done by the sum of applied and inertial forces (F_i and $m_i a_i$) in moving the body through a virtual distance δr_i. Since the forces sum to zero, no virtual work is said to be done. The inertial forces are calculated by considering an accelerating coordinate system attached to the centre of mass of the structure. The acceleration of the system is simply calculated by assuming rigid body motion (F = ma). The acceleration of each element is then obtained through geometry, and finally, the inertial forces for each element are then calculated. It may be noted that the applied forces do not necessarily need to be in equilibrium, since they will be balanced by inertial forces.

This analysis is useful in analysing suspension control arms, since they are free to rotate about the axis through their chassis mounts. Inertia relief analysis thus calculates the steady state stress and deformation in the structure as if it were accelerating under the applied forces [43]. Boundary conditions may be applied in order to constrain rigid body motion, but the reaction forces for these conditions will be equal to zero.

Chapter 4: Results

In this chapter, results obtained from the application of the terrain modelling and analysis methodology discussed in Chapter 3 are presented. Synthesised terrain profiles of different categories of terrain, generated using the autoregressive and Markov models are presented. The statistical properties of the profiles are discussed in detail in order to assess the performance of each terrain model in capturing the statistical properties of the measured terrain.

The performance of the terrain models is further assessed by studying how well they are able to capture vehicle excitation properties of the measured terrain. This assessment is done by comparing the estimated suspension component service life for the synthesised terrain and the measured terrain. For fatigue analysis, the acceptance criterion for correlation is widely regarded to be a factor of 3, and sometimes as high as an order of magnitude [44]. The spectral density plots of the terrain profiles are also helpful in comparing the vehicle excitation properties of the terrain pertinent to ride analysis. Before assessing the performance of the terrain models in modelling terrain, a study was done to determine the statistical closeness between two different terrain profiles from the same stretch of terrain (for example, the left and right wheel path profiles measured on the same stretch of terrain). This study indicated the sensitivity of the statistical methodology used in this work, to variations in statistically similar profiles, and was used to gauge the quantitative performance that could be expected of the terrain models. A similar study was done to establish the limits of correlation that can be expected from the fatigue analyses performed in this work. Fatigue lives corresponding to several profiles from the same stretch of terrain were compared in order to obtain the variation between them.

This chapter is divided into three parts. Part 1 presents the sensitivity and fatigue correlation limit studies performed on one set of terrain profiles. Part 2 presents the

application of terrain modelling and analysis to selected terrain data and Part 2 presents the statistical comparison between two different terrain datasets, using the statistical analysis methodology presented in chapter 3.

4.1 Statistical Sensitivity and Fatigue Correlation Studies

For the purpose of studying the sensitivity of the statistical methodology used in this work, to variations in what are expected to be statistically similar profiles (i.e. different profiles of the same stretch of terrain), terrain data from the Danville Airport auxiliary runway was used. The same dataset was used to establish the correlation limits of fatigue life estimations. The dataset consisted of 89 longitudinal terrain profiles containing 6932 elevation values interpolated at longitudinal distances of 25 mm spacing. Starting from the first profile, every 10^{th} profile was used in this study, 8 profiles total. The first profile was compared with every other profile under consideration (therein assuming that the first profile belonged to a particular stochastic process (i.e. a control realisation), and all other profiles were subsequent realisations of the same stochastic process; i.e. a sample set).

It was seen that in most of the statistical tests, the *p-values* (i.e. the probabilities that the statistical metric distributions of the sample terrain profiles matched those of the control profile) lay above the 95% confidence limit. The test of Gaussianity yielded low *p-values* and the null hypothesis (that the distributions belonged to realisations that originated from the same stochastic process) was rejected at the 95% confidence level. However, since all the profiles originated from the same sample terrain, they are therefore expected to be realisations of the same stochastic process. This fact was used to redefine the expected level of confidence according to the p-value calculated from the stated sample set.

The 85^{th} percentile *p-values* obtained from the sensitivity studies (rounded to the nearest order of magnitude) are summarised in Table 1. Assuming equal weighting to all statistical tests in calculating the *G-value*, *G-values* ranging between 0.6 and 0.7 were calculated for the sample set under consideration. The figures on the following page

show the distribution of the IRI and stationarity metrics for the left and right wheel paths in the DAP terrain data. It can be seen that there is slight variation in the IRI values calculated for the two profiles. The choice of terrain profile used for vehicle dynamics and durability studies would clearly have an effect on the outcome of the simulations, and no single profile can be seen to be representative of all other profiles in the same terrain section. This result provides an indication of what variability can be acceptable in order to classify synthesized terrain models as having successfully captured the statistical properties of the measured terrain profiles.

Table 1: 85th percentile *p-values* for sensitivity studies

Gaussianity	1.00E-14
Linearity	0.98
Stationarity	1.00
Time Invariance	0.735
IRI	0.11
RMS	0.98
Mean	0.98
Rainflow Count	0.37
Standard Deviation	0.73

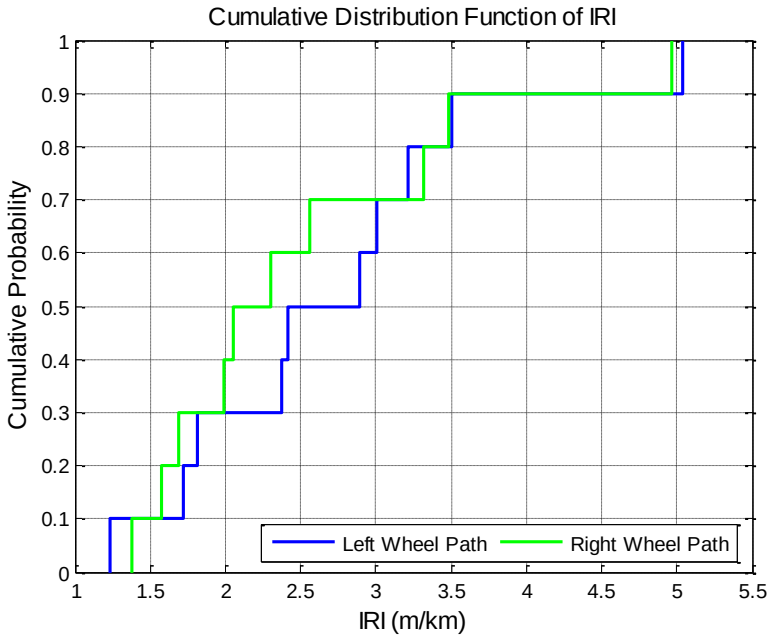

Figure 23: Distribution of IRI metrics for left and right wheel paths

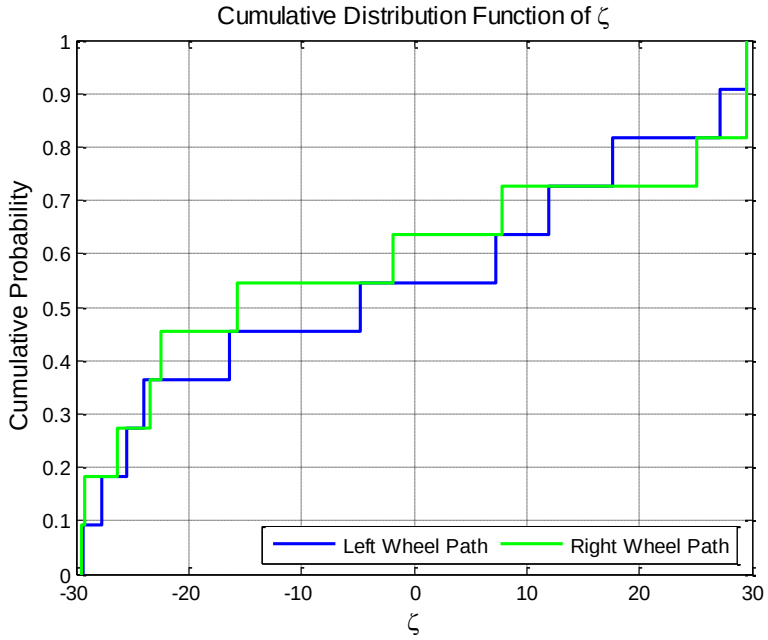

Figure 22: Distribution of values of ζ for left and right wheel paths

The profiles discussed above were then used to obtain fatigue life estimations for the front lower control arm of the Jetta. It was seen that the variations in fatigue life predictions, as expected, were up to an order of magnitude. Thus, the correlation limits for fatigue life predictions can be assumed to be an order of magnitude for this type of terrain (i.e. smooth asphalt). Table 2 provides a summary of fatigue life predictions for several sample terrain profiles.

Table 2: Summary of G-values and fatigue life estimations for DAP profiles

Profile	1st	10th	21st	31st	41st	51st
G-value	-	0.2178	0.14032	0.1371	0.152	0.1753
Fatigue Life (cycles)	4.225E+04	3.29E+05	6.40E+05	6.31E+05	9.486E+03	2.28E+05

From the values tabulated above, it was observed that there was no correlation observed between the *G-value* and the fatigue life predictions as expected. Neither was there any correlation between any statistical metric *p-value* and the *G-value*. However, as shown in section 4.3, there was some indication of such correlation in the case of the unpaved terrain and proving ground course discussed subsequently in this chapter.

4.2 Application of Terrain Modelling to Selected Terrain Data

The terrain modelling methodologies discussed previously have been applied to measured terrain datasets of selected types. Three different terrain types have been dealt with in this work; namely U.S. highway roads, unpaved roads and courses typically found in vehicle durability proving ground facilities. In this section, terrain profiles synthesised using the AR and Markov models are presented, along with an assessment of their performance in capturing the properties of the measured terrain. All results shown here are representative of typical results obtained using these methods.

4.2.1 Bump-and-pothole proving ground course

The terrain profile shown in Figure 24 (a) is a representation of a typical bump-and-pothole course that is maintained by most automobile manufacturers at their proving ground facilities. It consists of randomly arranged speed bumps and troughs on an underlying flat terrain which serve to provide extreme excitation to a vehicle, especially chassis and suspension systems, in order to perform tests such as an accelerated durability test (ADT). An example of the corresponding terrain profiles generated using the AR and the Markov models are shown in Figures (b) and (c). For visual clarity, only a 10 metre section of each profile has been shown in this figure. Visually, the Markov-synthesised profile can be seen to contain distinct bumps and potholes of varying size and distribution, on flat terrain. This result can provide a useful random character to the otherwise deterministic course, while maintaining its basic character, leading to durability results which have a more generic rather than specific scope. The AR-synthesised profile has a more overall rough character, although distinct bumps and potholes can be seen.

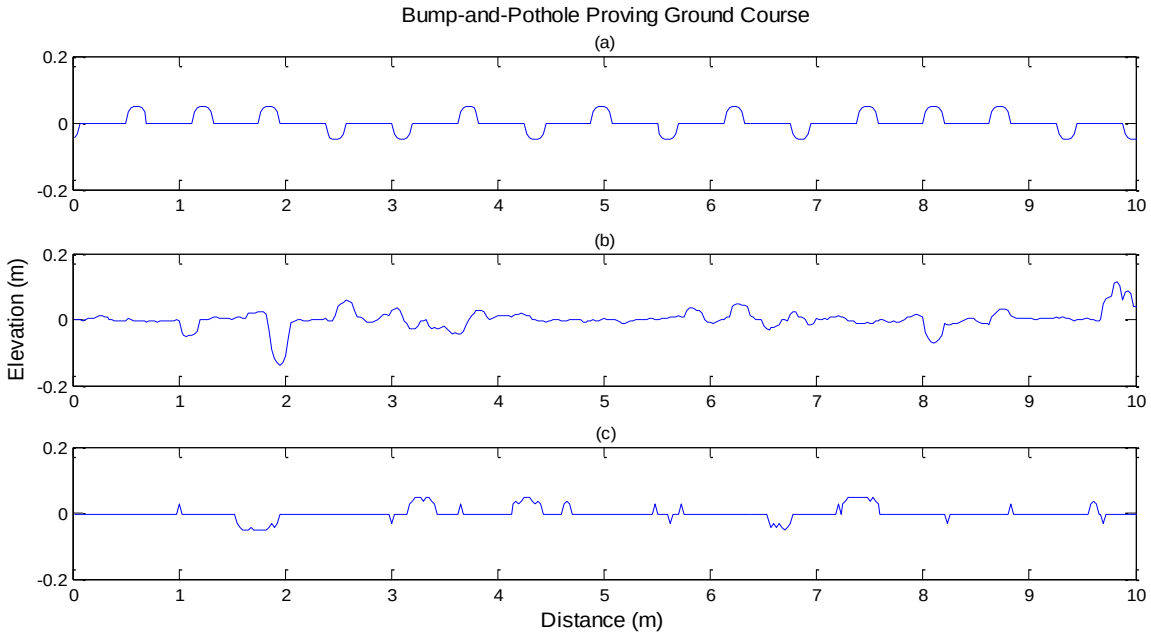

Figure 24: Proving ground course profiles:
(a) Representation of typical bump-and-pothole proving ground course
(b) AR-synthesised profile (c) Markov-synthesised profile

Statistical analysis of the profiles shows that the distributions of the International Roughness Index (IRI) shows that the variation in the IRI of the measured data is much smaller than the variation in synthetic profiles generated by either model. The cumulative distribution plot (CDF) of the IRI values calculated in 15 m sections is shown in Figure 25. This is demonstrated by small range of IRI between 34 and 39 m/km. Both the AR-synthesised and Markov-synthesised profiles show much greater variation. In addition, the data synthesized from the Markov chain is much smoother (having significantly lower IRI values) than the other two.

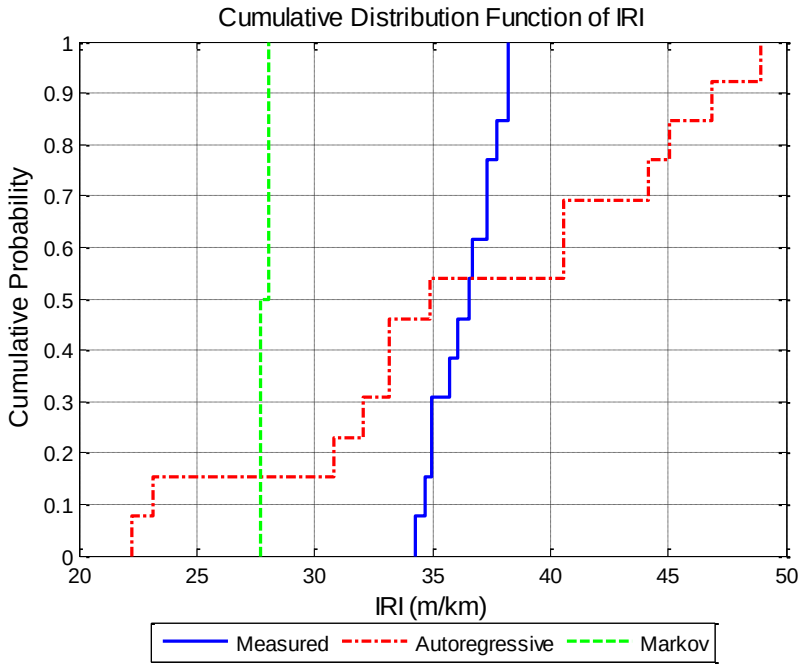

Figure 25: Distribution of IRI for proving ground course

The distributions of the rainflow count (Figure 26) indicate that the Markov-synthesised profile conforms to the original profile much more than the AR-synthesised profile does in terms of the number of closed-loop cycles. However, neither models produced profiles with distributions of rainflow count close to that of the original profile. Similarly, the distributions for stationarity, Gaussianity and time invariance for the Markov-synthesised profile lie close to those for the original profile, indicating that the Markov model is possibly more successful at modelling this type of terrain.

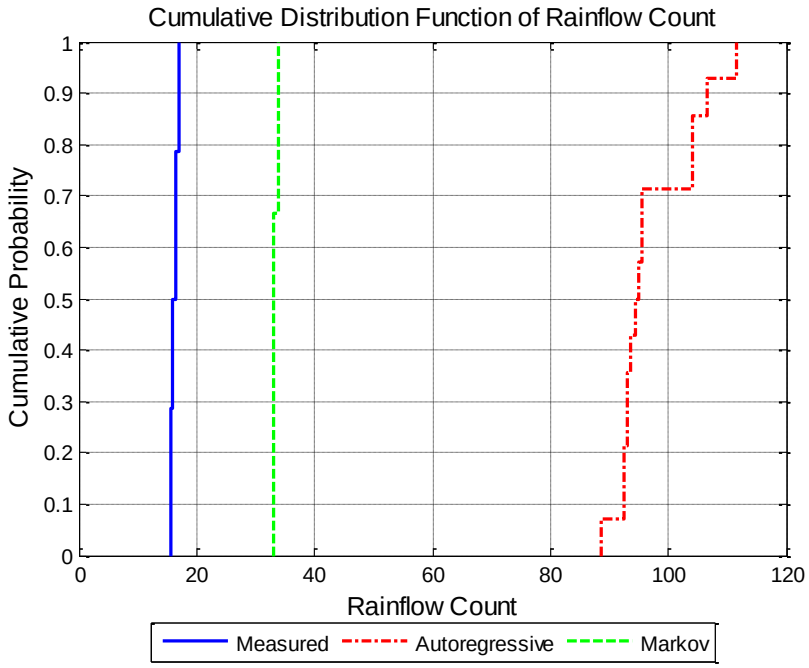

Figure 26: Distribution of rainflow count for proving ground course

The *p-values* for the different statistical metrics for this example are summarised in Table 3. Since the metric distributions do not coincide to a great extent, the p-values are all low in value, leading to low *G-values*. These *G-values* (calculated with equal weighting for all metrics) indicate that the Markov-synthesised profile performed better at conforming to the metric CDFs as compared to the Markov-synthesised profile. The overall values of the statistics for the profiles are summarised in Table 4.

Table 3: Statistical p-values for proving ground course

	AR	Markov
Gaussianity	0	0
Linearity	0.003	0.004
Stationarity	2.8E-07	0.04
Time Invariance	2.8E-07	0.36
IRI	0.087	0.02
Rainflow Count	2.8E-07	0.004
Standard Deviation	0.003	0.004
G-value	**0.040**	**0.144**

Table 4: Statistical property values for proving ground course

	Units	Original	AR	Markov
Gaussianity (D_n)	-	0.363	0.124	0.422
Linearity (F)	-	0.350	0.958	12.268
Stationarity (ζ)	-	-36.619	0.652	-40.808
Time Invariance (p_{ti})	-	0.854	0.502	0.856
IRI	m/km	35.6	35.2	30
Rainflow Count	-	58.5	356.5	120.5
Standard Deviation	mm	22.912	25.563	18.898

The Spectral density plots of the three profiles (assuming a vehicle speed of 50 km/h) are shown in Figure 27. It can be seen that the spectral content of the synthesised profiles are near the same order of magnitude of the original profile.

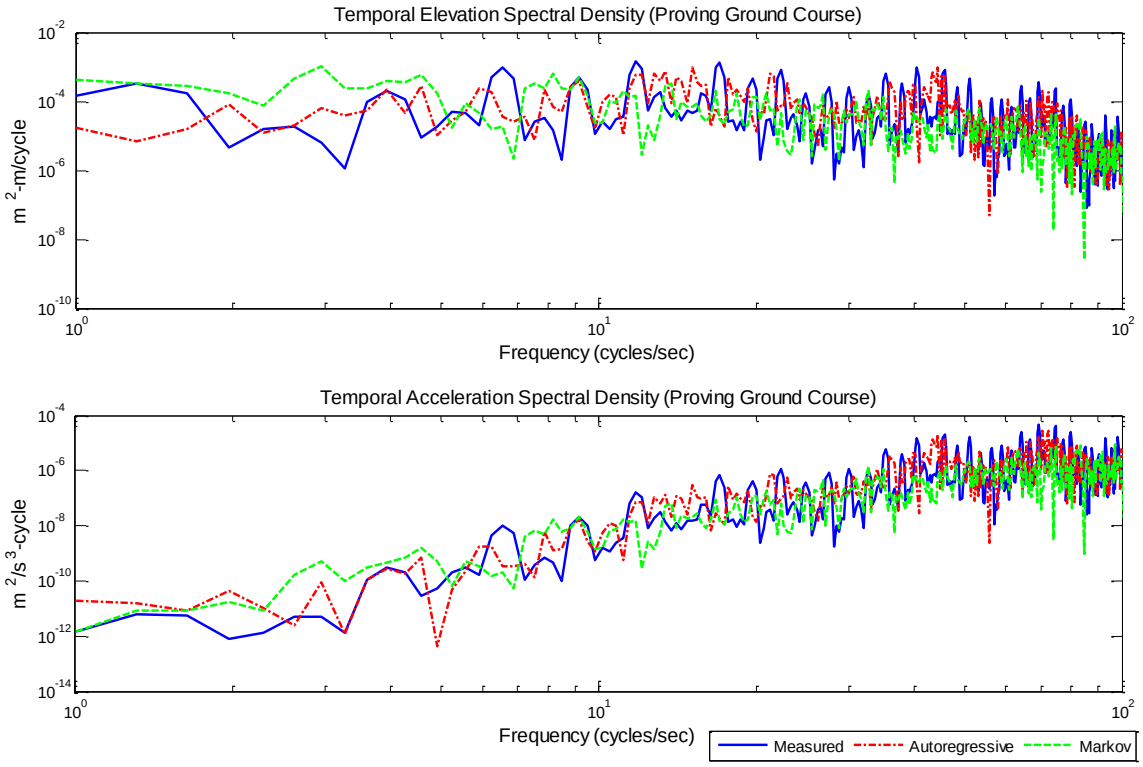

Figure 27: Spectral density plots of proving ground course

The final method of assessing the performance of the models is comparing the estimated fatigue life (i.e. cycles-to-crack-initiation) of the suspension components. The front LCA of the Jetta was subjected to the loading histories obtained for all three profiles, and the fatigue lives were calculated as shown in Table 5. These numbers are for a course of 55 m length. Thus, it can be seen that the AR model can be said to have performed better in capturing the suspension fatigue inducing properties of the original profile, since the fatigue life corresponding to this model correlates better with the life calculated for the original profile. The fatigue life for the Markov-synthesised profile was greater than a factor of 5, and thus the Markov model can be said to have modelled this terrain unsuccessfully from a vehicle excitation point of view, although visually it was seen to successfully recreate the bumps and potholes of the original profile.

Table 5: Fatigue life of Jetta front LCA for proving ground course

Measured	AR	Markov
6.979E+02	9.698E+02	2.331E+03

4.2.2 U.S. highway terrain

The terrain profile shown in Figure 28 (a) is a part of the profile from the Federal Highway Administration's (FHWA) Long Term Pavement Performance (LTPP) program. This data has been collected from a section of the US-280 highway. The corresponding terrain profiles generated using the AR and the Markov models are shown in Figures (b) and (c). For visual clarity, only a 10 metre section of each profile has been shown in this figure. Visually, both the synthesised profiles contain features similar to that of the measured profile. However, the Markov-synthesised profile contains more severe features. This can be verified statistically by observing the distribution of IRI of the profiles in Figure 29, where the Markov-synthesised terrain has consistently higher IRI compared to the other two profiles. However, the Markov model fared better at conforming to the distribution of linearity of the measured profile, as seen in Figure 28.

.

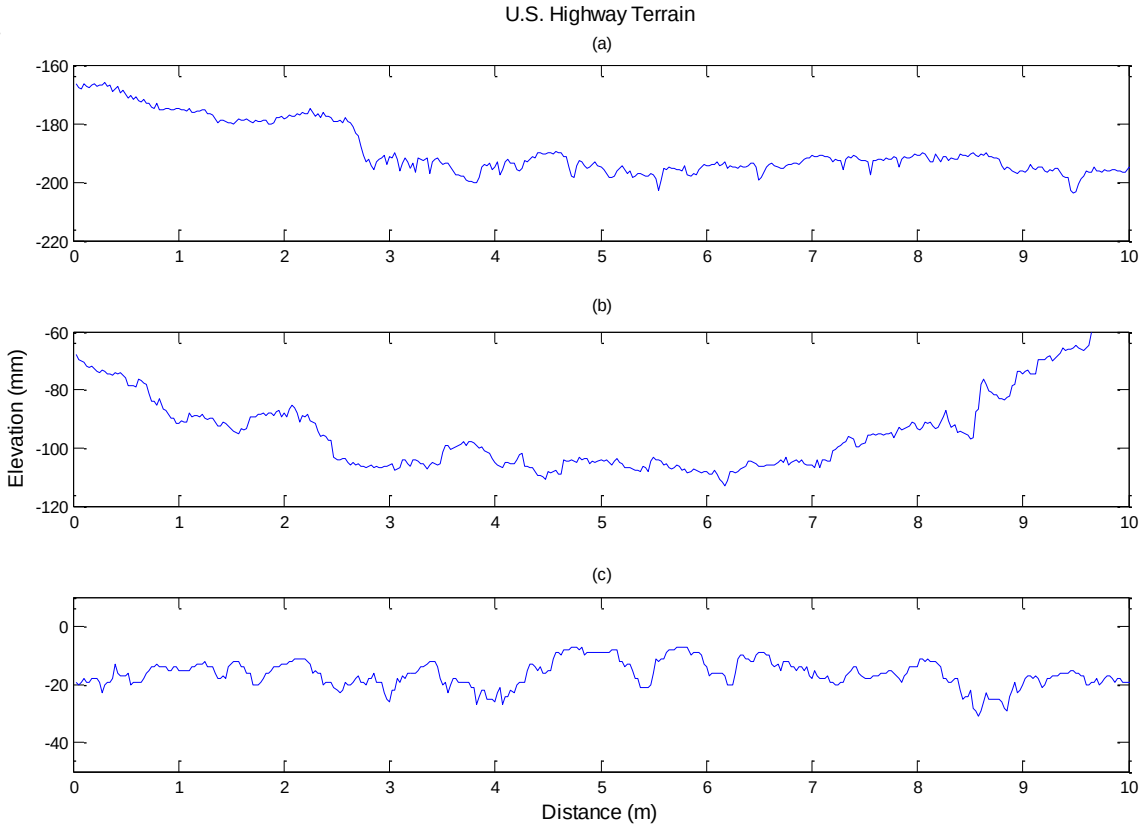

Figure 28: U.S. highway profiles: (a) Measured terrain profile (b) AR-synthesised profile (c) Markov-synthesised profile

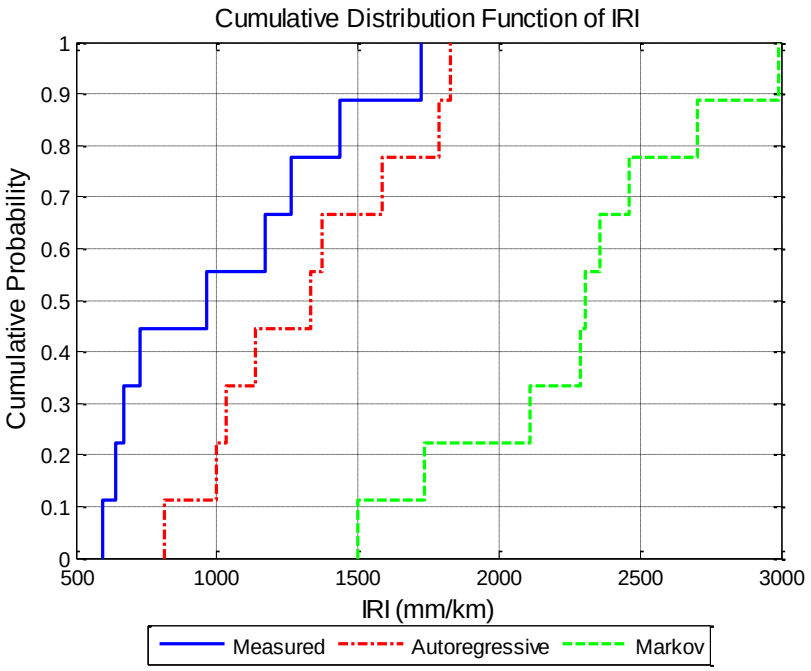

Figure 29: Distribution of IRI for U.S. highway terrain

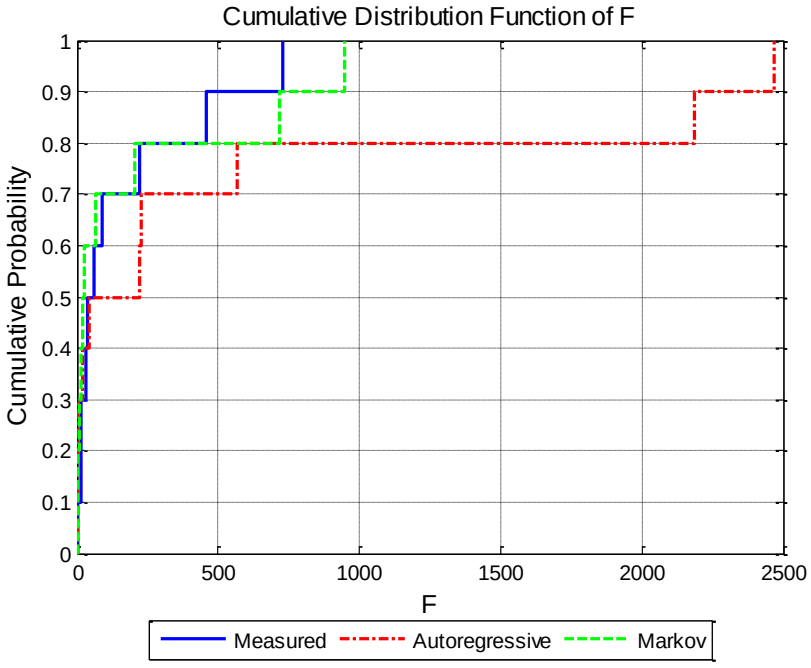

Figure 30: Distribution of linearity for U.S. highway terrain

This is an unexpected result, since the AR model is linear by construction, and therefore must be linear. This is perhaps an of a Type II error (i.e. a false negative, in which the terrain profile was classified as non-linear when in reality, it was linear). The *p-values* for the different statistical metrics are summarised in Table 6. Since some of the metric distributions did coincide to a good extent, the corresponding p-values are high in value, leading to high *G-values*. These *G-values* indicate that both the models performed equally well at conforming to the metric CDFs of the measured profile. The overall values of the statistics for the profiles are summarised in Table 7.

Table 6: Statistical p-values for U.S. highway terrain

	AR	Markov
Gaussianity	1.65E-33	0.0161
Linearity	0.675	0.675
Stationarity	0.11	0.11
Time Invariance	0.675	0.97
IRI	0.25	4.9E-04
Rainflow Count	0.11	1.88E-05
Standard Deviation	0.031	0.675
G-value	**0.42**	**0.45**

Table 7: Statistical property values for U.S. highway terrain

	Units	Original	AR	Markov
Gaussianity (D_n)	-	0.075	0.063	0.075
Linearity (F)	-	90.38	8.37	25.98
Stationarity (ζ)	-	-4.19	30.78	0.68
Time Invariance (p_{ti})	-	0.44	0.50	0.46
IRI	m/km	1.127	1.325	2.449
Rainflow Count	-	1552	1503	1231.5
Standard Deviation	mm	2.98	2.58	3.17

The Spectral density plots of the three profiles (assuming a vehicle speed of 50 km/h) are shown in Figure 31. It can be seen that the spectral content of the AR-synthesised profile matches that of the original profile to within an order of magnitude. However, the spectral density of the Markov-synthesised profile is consistently higher through the lower range of frequencies of interest, indicating more severe events in the lower frequency bandwidth. Thus, the AR model can be said to be more successful in capturing the characteristics of the terrain pertinent to vehicle ride than the Markov model.

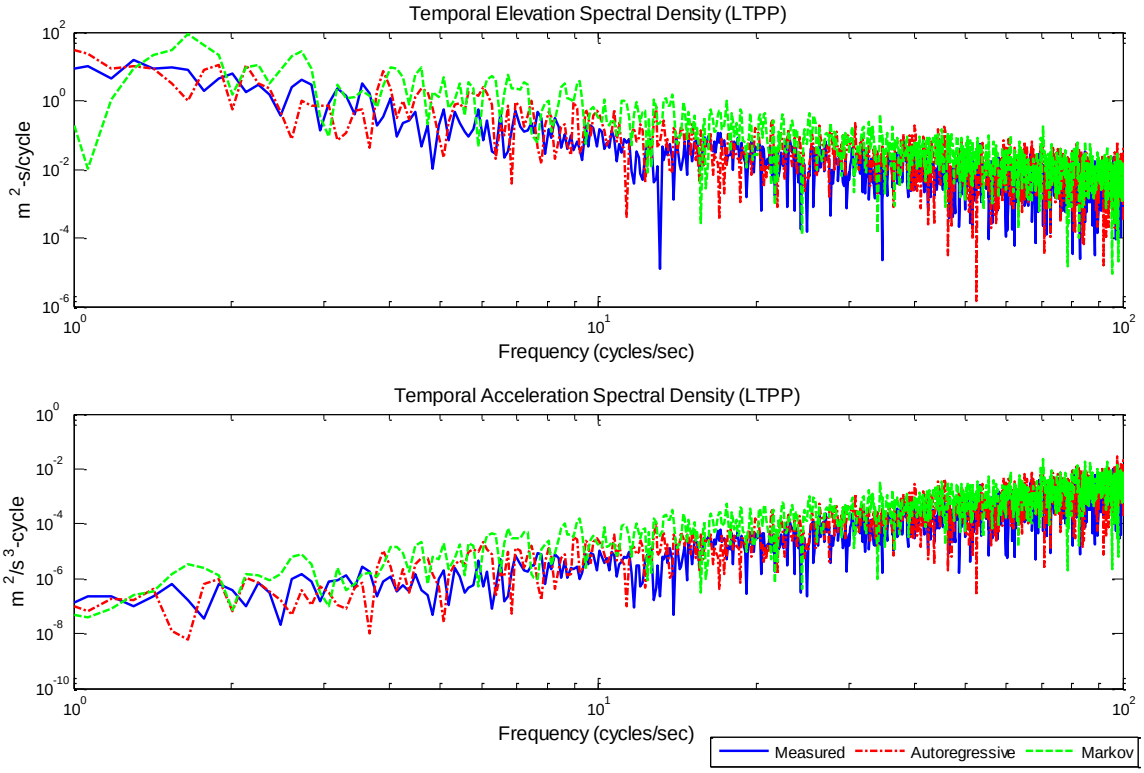

Figure 31: Spectral content of the profiles for U.S. highway terrain

The final method of assessing the performance of the models is comparing the estimated fatigue life (i.e. cycles-to-crack-initiation) of the suspension components. The front LCA of the Jetta was subjected to the loading histories obtained for all three profiles, and the fatigue lives were calculated as shown in Table 8. These numbers are for a course of 152.5 m length. Thus, it can be seen that the AR model can be said to have performed better in capturing the suspension fatigue inducing properties of the original profile, since the fatigue life corresponding to this model correlates better with the life calculated for the original profile. However, the Markov model was successful in this regard too, since the fatigue life predicted was within a factor of 5. The entire terrain profiles for the U.S. highway data are shown in Figure 32.

Table 8: Fatigue life of Jetta front LCA U.S. highway terrain

Measured	AR	Markov
6.554E+07	5.797E+07	9.912E+06

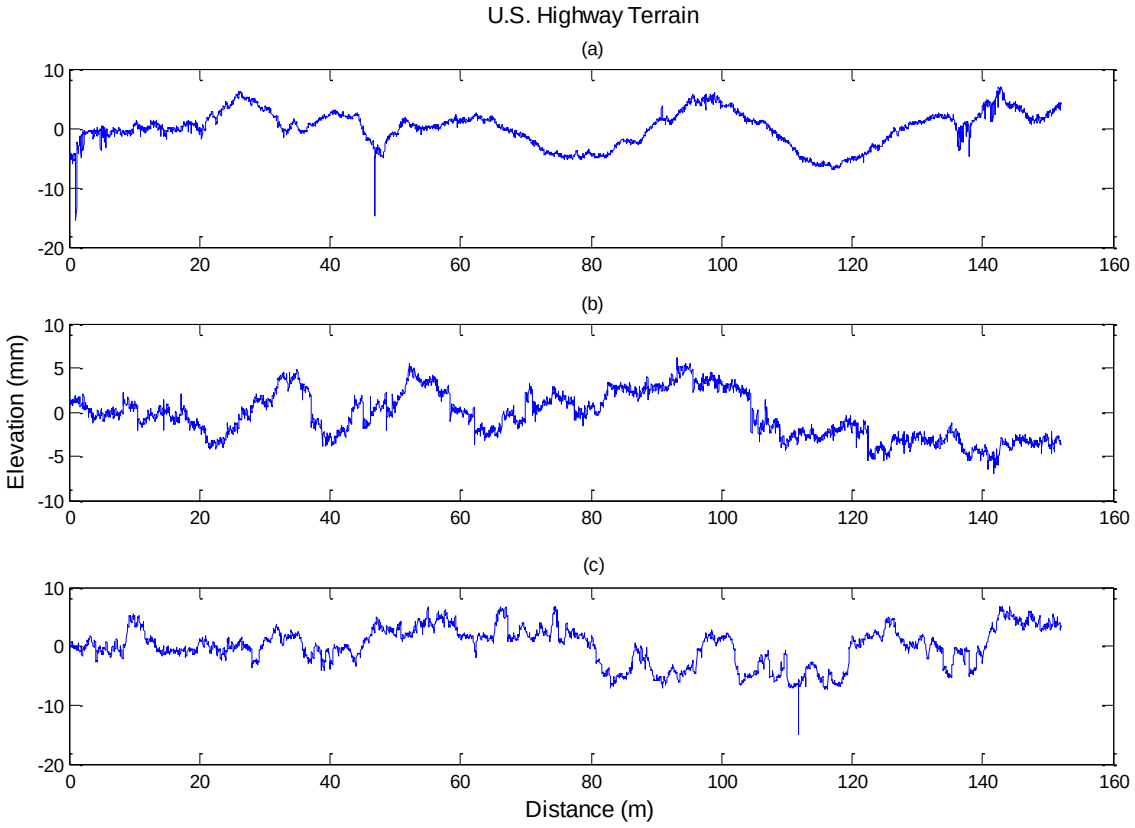

Figure 32: Terrain profiles for U.S. highway terrain

4.2.3 Unpaved terrain

The terrain profile shown in Figure 33 (a) is a section from an unpaved access road to the regional airport in Danville, VA. As can be seen from the plot of the entire profile in Figure 34, the profile contains severe undulations. The corresponding terrain profiles generated using the AR and the Markov models are shown in Figures (b) and (c). For visual clarity, only a 10 metre section of each profile has been shown in this figure. At the scale shown in Figure 33, both the synthesised profiles contain features similar to that of the measured profile. However, as can be seen in the full-scale profiles in Figure 34, the Markov-synthesised profile fails to capture the long-wavelength undulations in the profile, which are captured by the AR-synthesised profile. This failure of the Markov model to capture the long-wavelength undulations may be a result of the regularly spaced binning and is discussed in more detail in the conclusions.

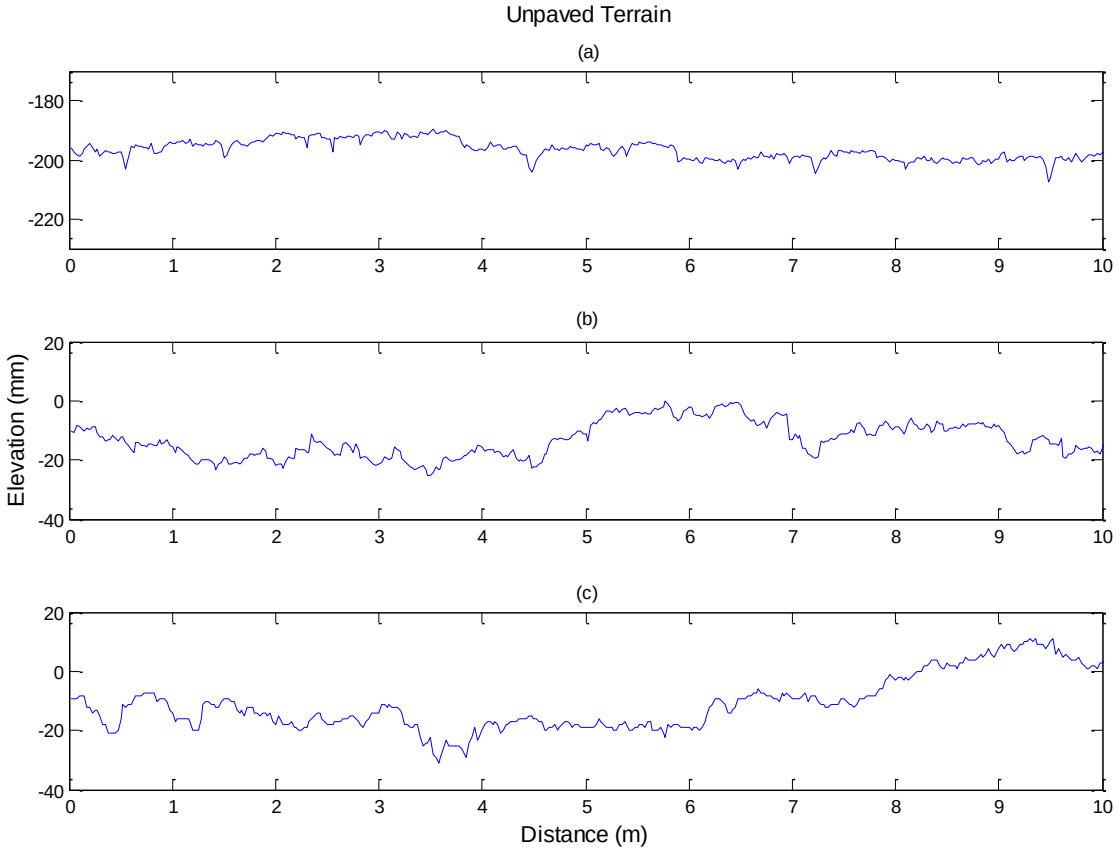

Figure 33: Unpaved terrain profiles: (a) Measured terrain profile (b) AR-synthesised profile (c) Markov-synthesised profile

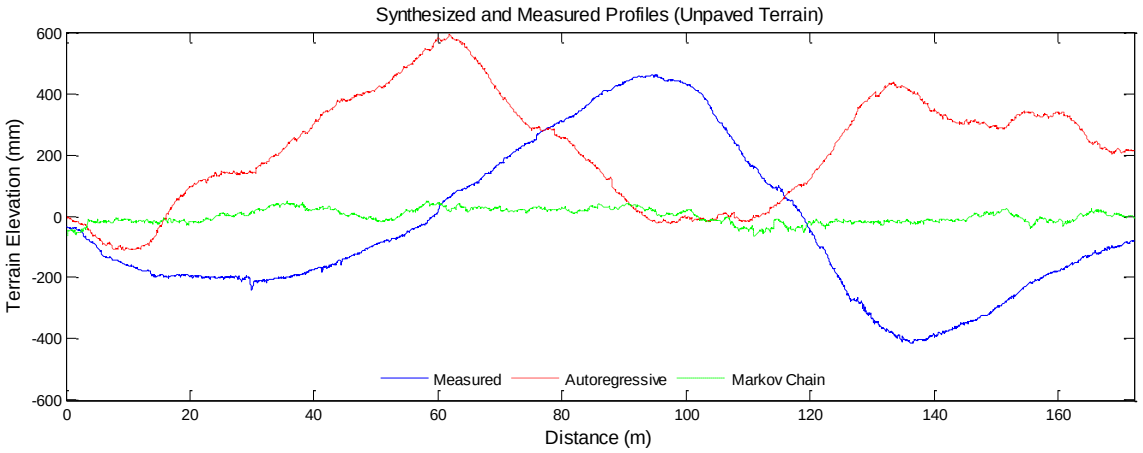

Figure 34: Unpaved terrain - synthesised and measured profiles

From the distribution of IRI shown in Figure 35, it can be seen that both the models generated profiles with a smaller range of roughness levels as compared to the measured profile, which contained smoother as well as rougher sections.

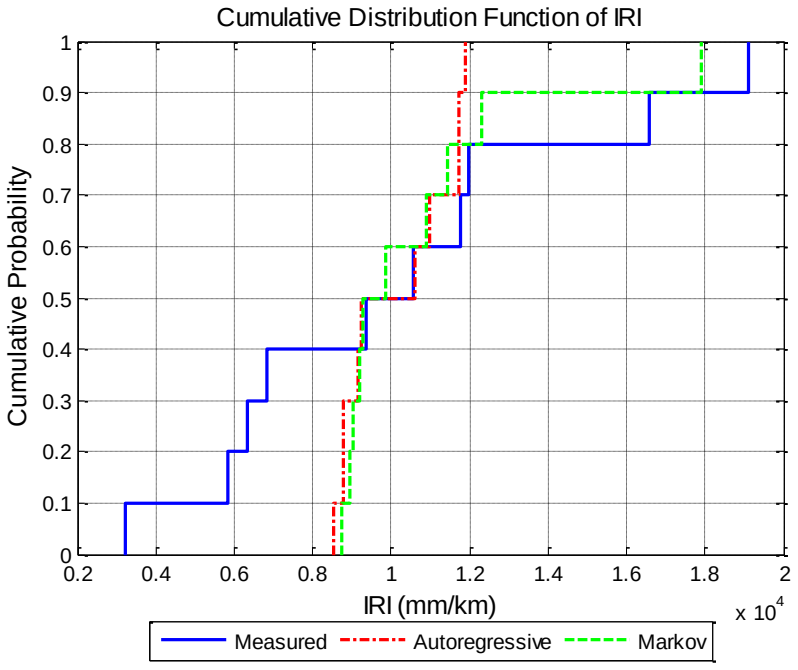

Figure 35: Distribution of IRI for unpaved terrain profiles

The *p-values* for the different statistical metrics are summarised in Table 9. Since some of the metric distributions do not coincide to a great extent in the case of the Markov-synthesised profile, the corresponding p-values are low in value, leading to low *G-values*. The *G-values* indicate that the AR model performed significantly better than the Markov model at conforming to the metric CDFs of the measured profile. The overall values of the statistics for the profiles are summarised in Table 10

Table 9: Statistical p-values for unpaved terrain

	AR	Markov
Gaussianity	9.66E-110	4.161E-61
Linearity	0.98	0.37
Stationarity	0.37	0.046
Time Invariance	0.73	0.37
IRI	0.31	0.31
Rainflow Count	0.046	5.9E-05
Standard Deviation	0.98	5.9E-05
G-value	**0.468**	**0.124**

Table 10: Statistical property values for unpaved terrain

	Units	Original	AR	Markov
Gaussianity (D_n)	-	0.1607	0.09	0.0941
Linearity (F)	-	0.0326	0.0969	1.03
Stationarity (ζ)	-	-7.09	-22.53	8.2
Time Invariance (p_{ti})	-	0.6382	0.4694	0.5075
IRI	m/km	8.68	12.23	11.29
Rainflow Count	-	1701	1614	1135
Standard Deviation	mm	253.96	181.01	23.07

The Spectral density plots of the three profiles (assuming a vehicle speed of 50 km/h) are shown in Figure 36. It can be seen that the spectral content of the synthesised profiles matches that of the original profile consistently. Thus, both models can be said to be successful in capturing the characteristics of the terrain pertinent to vehicle ride.

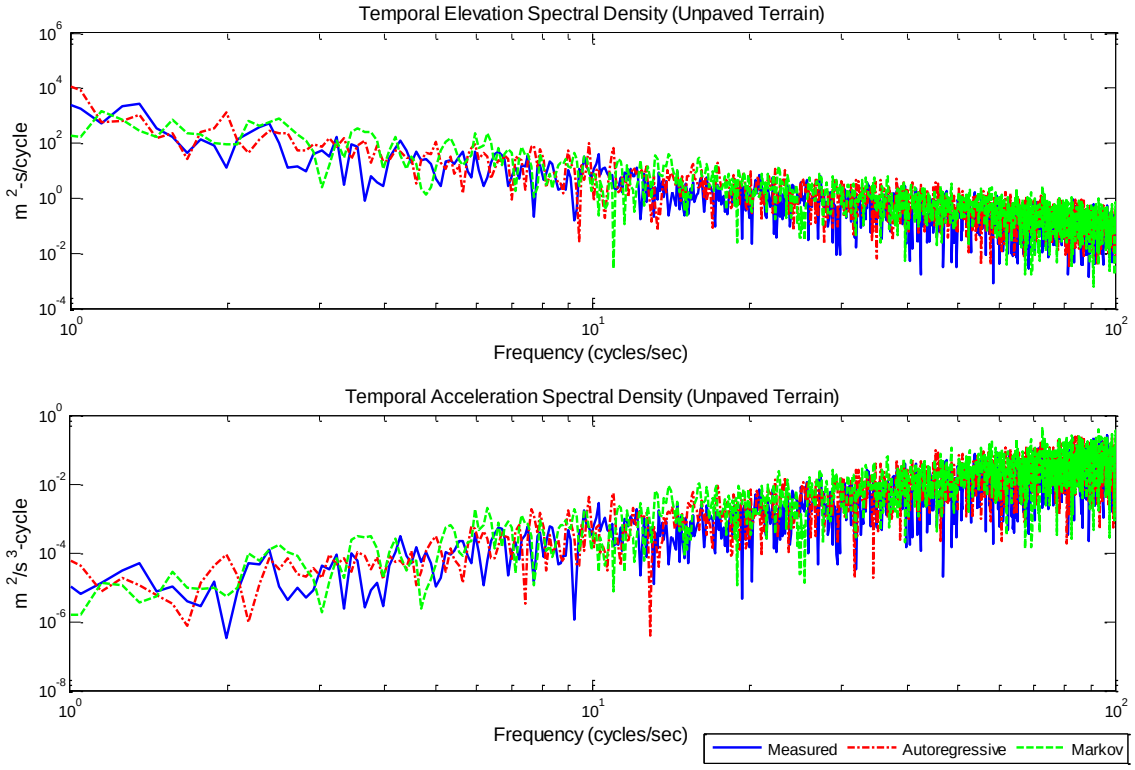

Figure 36: Spectral density plots of unpaved terrain

The final method of assessing the performance of the models is comparing the estimated fatigue life (i.e. cycles-to-crack-initiation) of the suspension components. The front LCA of the Jetta was subjected to the loading histories obtained for all three profiles, and the fatigue lives were calculated as shown in Table 11. These numbers are for a course of 171.5 m length. Thus, it can be seen that the AR model can be said to have performed better in capturing the suspension fatigue inducing properties of the original profile, since the fatigue life corresponding to this model lies within a factor of 5 of the life calculated for the original profile. The Markov model can be said to have been

unsuccessful in modeling this terrain since the corresponding fatigue life did not correlate well with that for the measured profile.

Table 11: Fatigue life of Jetta front LCA for unpaved terrain

Measured	AR	Markov
2.423E+04	7.028E+03	1.691E+07

4.3 Using Statistical Analysis Methodology to Compare Different Terrain

In this section, the terrain profile analysis methodology described in the sections above is applied to statistically compare two different terrain profile samples. The intent is to investigate the applicability of the method to compare profiles of different types of terrain, in order to see how close in agreement their statistical properties are. The final goal of this comparison is to identify how statistical properties can be used to group terrain into different types – e.g. tarmac (smooth or rough), gravel, highway (recently paved or degraded) etc. Terrain profiles from the Danville Airport auxiliary runway and the LTPP data (Figure 37) have been compared in this section. Some brief conclusions can be made from the results.

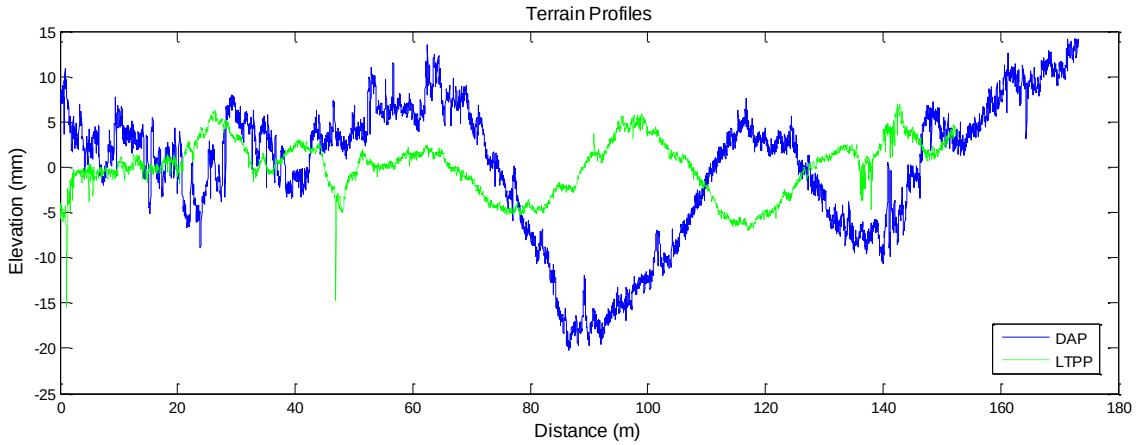

Figure 37: DAP and LTPP terrain profiles

The distribution plot for Keenan's statistic *F* for linearity (Figure 38) indicates that when analysed at a smaller scale, the LTPP profile has more linear characteristics compared to the DAP profile. When analysed as a whole however, the DAP profile was shown to have more linear properties, as indicated by a lower *F-statistic*. In Figure 39, (a) shows the section of the DAP profile which has highest linear characteristics, while the section shown in (b) shows the most non-linear section.

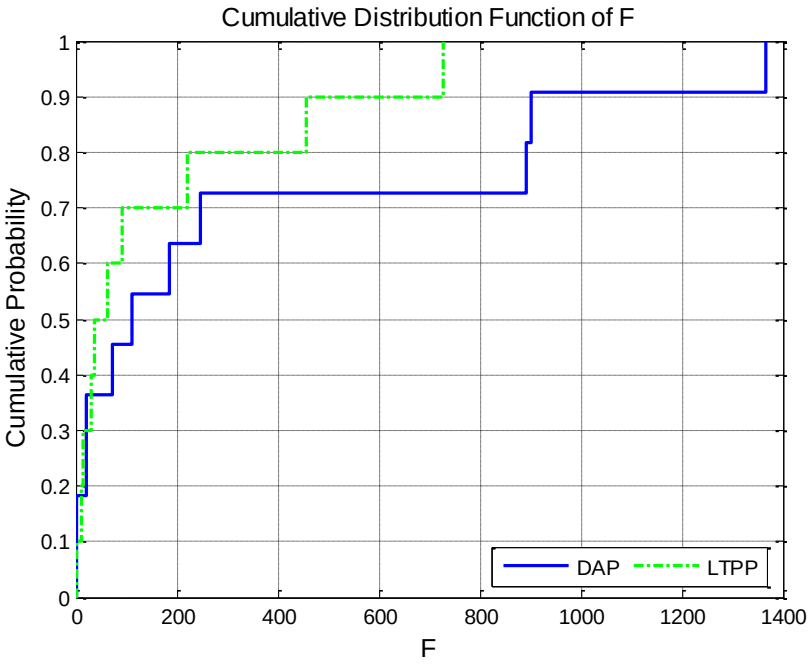

Figure 38: Distribution of linearity in the LTPP and DAP profiles

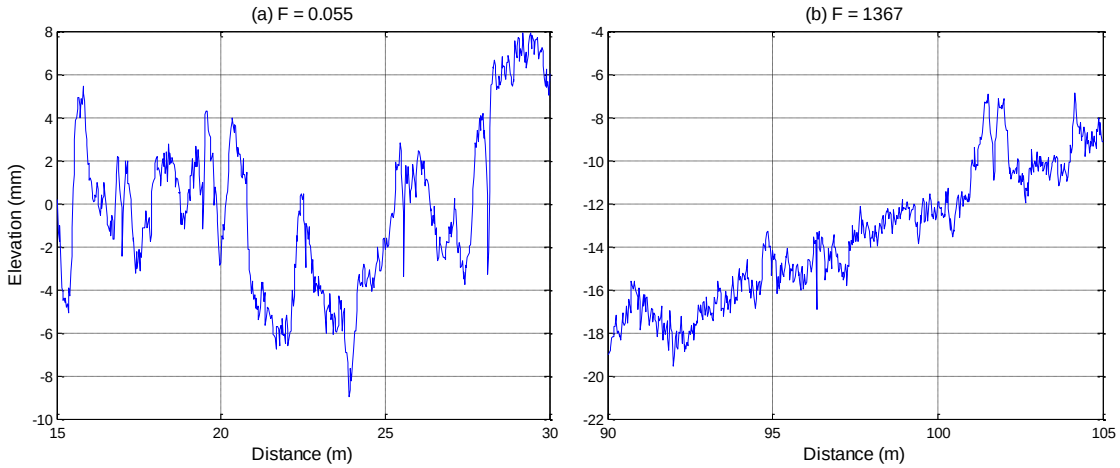

Figure 39: Linearity of DAP profile - (a) Section of DAP profile having highest linearity (b) Section of DAP profile having least linearity

The distribution of ζ (Figure 40) indicates that the LTPP profile has a higher probability of being stationary compared to the DAP profile, since the values of ζ are closer to the confidence limit bounds in the case of the LTPP data. This is corroborated by the absolute values of ζ for the two profiles.

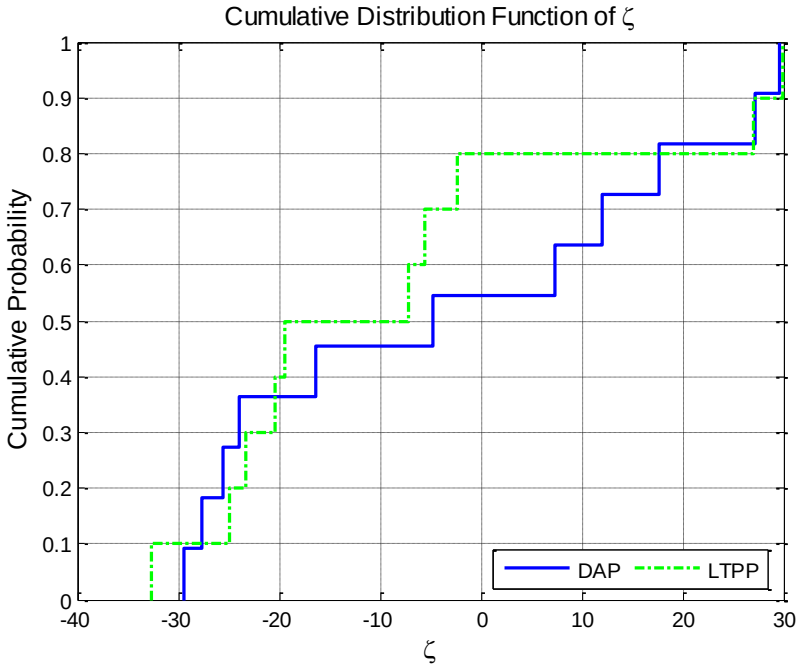

Figure 40: Distribution of stationarity for DAP and LTPP profiles

From the distribution of time invariance (Figure 41), it can be concluded that the LTPP profile has greater probability of being time invariant since the distribution curve of p_{ti} lies closer to the 0.5 value. This conclusion concurs with the previous conclusion that the LTPP profile has a higher probability of being stationary since the two properties are closely related.

The plot of IRI (Figure 42) clearly indicates that the DAP profile is consistently rougher than the LTPP profile. From Table 12, it can be seen that the DAP profile has a higher overall IRI value, indicating higher overall roughness. From the distribution of IRI metrics, rough and smooth sections can be isolated based on the local IRI values. Figure 43 (a) shows the section of the LTPP profile having the least IRI (1.35 m/km) –

this corresponds to the smoothest section of the profile. Figure 43 (b) shows the roughest section which has an IRI of 4.4 m/km. Clearly, this section contains more large magnitude disturbances compared to the section shown in (a). The variation of local IRI values throughout the profile is shown in Figure 44.

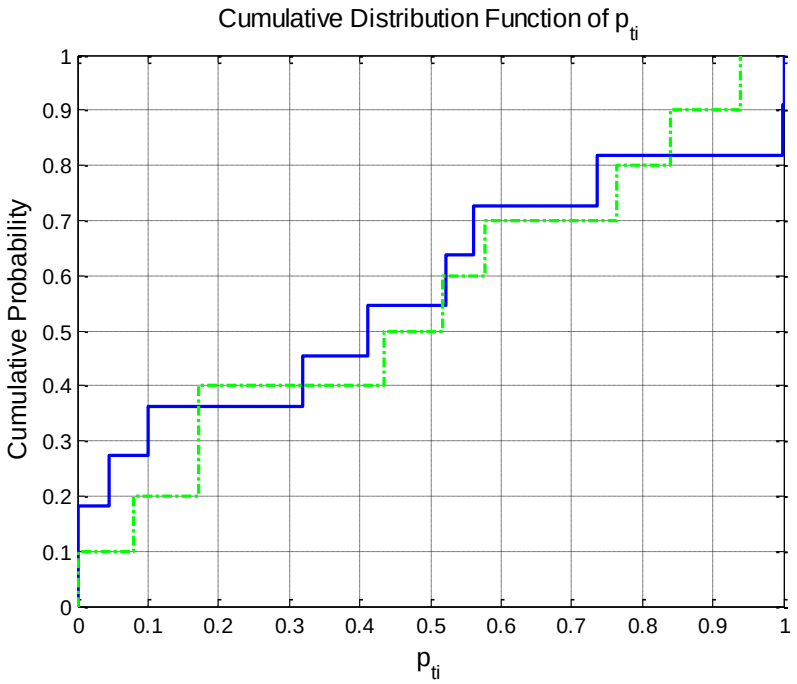

Figure 41: Distribution of time invariance for DAP and LTPP profiles

The rainflow count statistic concurs with the IRI statistic in characterising the DAP profile as being rougher. This is indicated by a higher rainflow count in the case of the DAP profile. It is to be noted however, that the rainflow count tends to characterise high frequency roughness (having wavelength of less than 1 metre), while the IRI filters this content out and characterises low frequency roughness (having a wavelength of 1 – 30 m).

These findings are supported by analysis of the spectral content of the two profiles. The elevation spectral density plots (assuming a vehicle speed of 50 km/h) shown in Figure 45 indicates that compared to the LTPP profile, the DAP profile has higher magnitude of content throughout the spectral range.

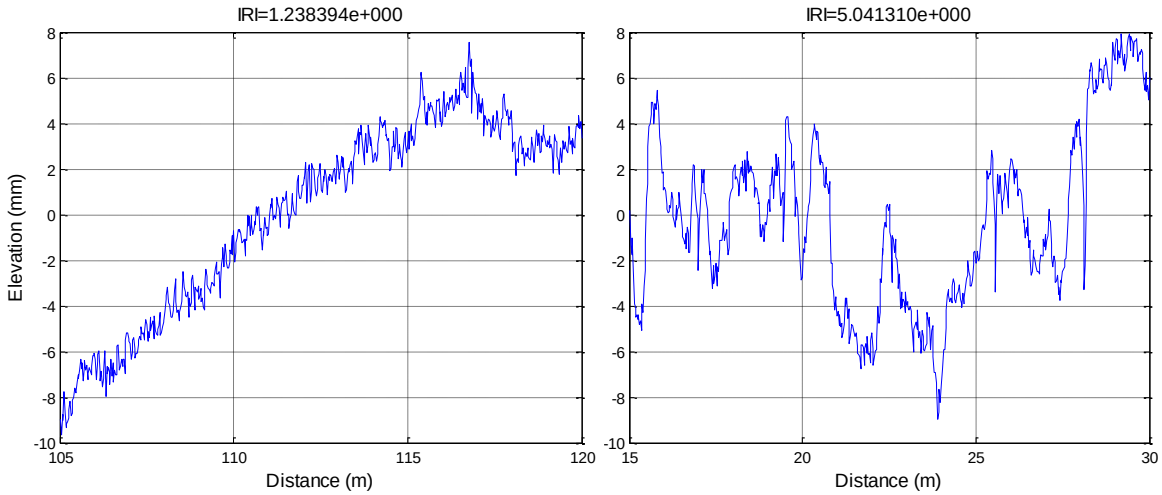

Figure 43: IRI in DAP profile: (a) Section of DAP having lowest IRI (b) Section of DAP having highest IRI

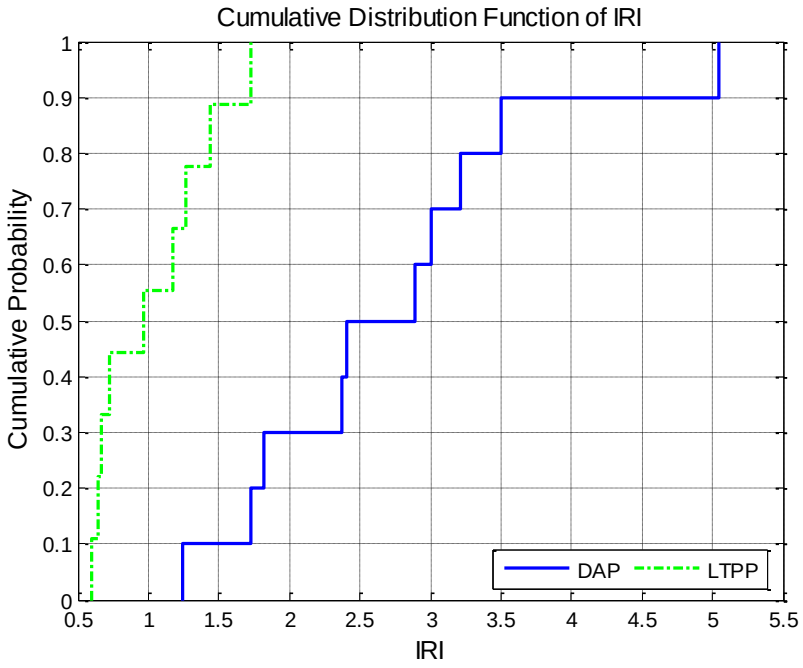

Figure 42: Distribution of IRI in the DAP and LTPP profiles

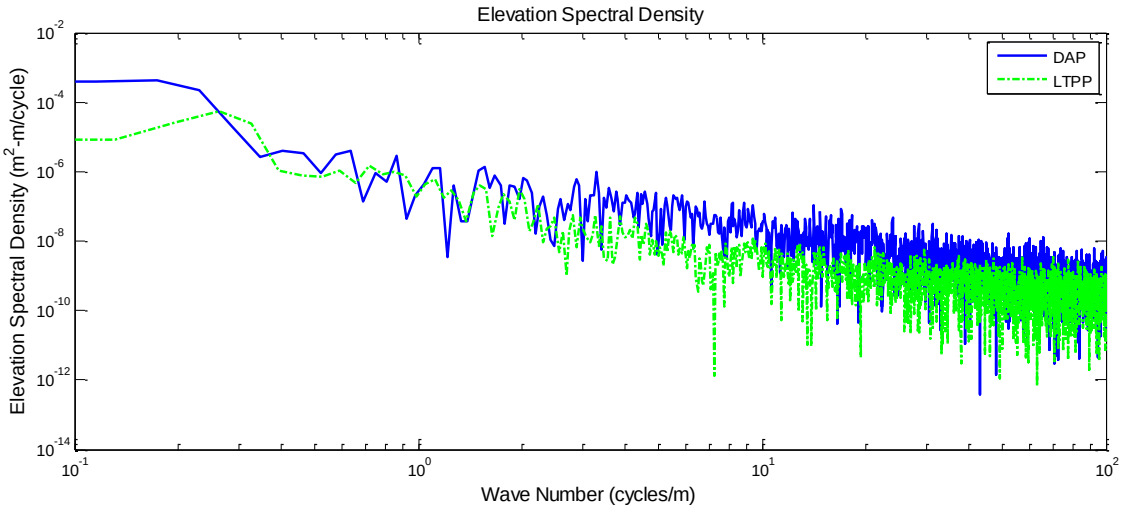

Figure 45: Spectral density of LTPP and DAP profiles

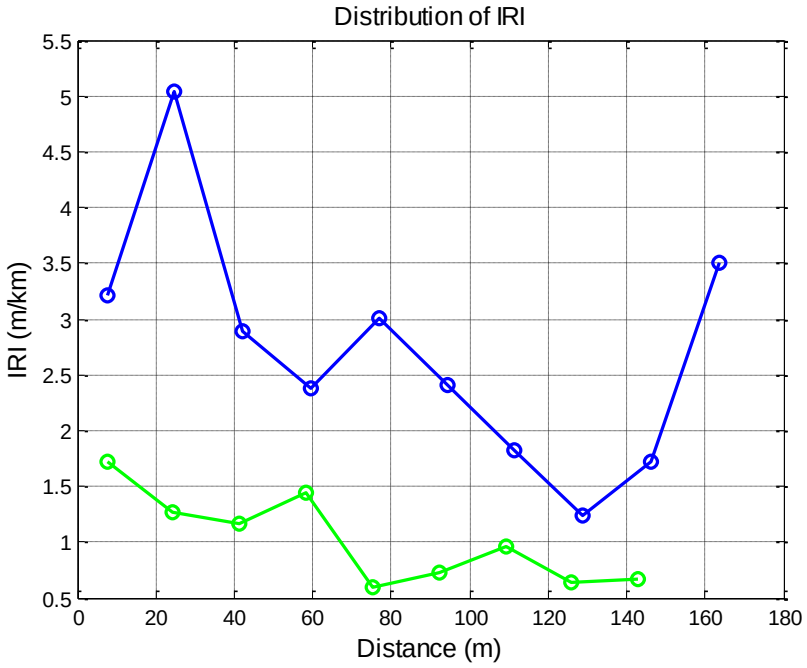

Figure 44: Variation of IRI in DAP and LTPP profiles

Table 12: Overall statistical metrics for DAP and LTPP profiles

Statistic	Units	LTPP	DAP
Gaussianity (D_n)	-	0.0749	0.1836
Linearity (F)	-	90.3854	0.6798
Stationarity (ζ)	-	-4.196	-13.538
Time Invariance (p_{ti})	-	0.53	0.39
IRI	m/km	1.786	2.447
Rainflow Count	-	1352	1919
Std. Deviation (σ)	mm	2.89	7.47

Chapter 5: Conclusions

5.1 Summary of Results

In chapter 4, the terrain modelling and analysis methodologies discussed in chapter 3 were applied to measured terrain data sets. Three main categories of terrain were evaluated viz. a bump-and-pothole proving ground course, U.S. highway roads, and an unpaved road. The performance of both AR and Markov chain models in capturing the physical and statistical properties of the measured terrain data were then assessed using two methods. First, a statistical goodness-of-fit parameter (*G-value*) of the synthesised terrain with the measured terrain was obtained. Secondly, the fatigue life (cycles-to-crack-initiation) of a suspension control arm was calculated for each terrain profile, as the vehicle model was made to traverse the terrain profiles. The following brief conclusions can be made from the results that have been presented in this work:

1. The average statistical goodness-of-fit values (*G-value*) that were calculated for both AR and Markov-synthesised profiles were much lower than expected (<0.1). This result implies that the AR and Markov chain models were inadequate in capturing the statistical properties of the measured terrain. This is probably due to the underlying assumption of stationarity that these models require. Due to the nonstationary nature of the terrain profiles, the AR and Markov models were unable to capture their statistical properties accurately. However, the low *G-values* notwithstanding, a comparison can still be made between the performances of the terrain models in simulating terrain. Table 13 shows a comparison of average *G-values* calculated for the AR and Markov chain models for the terrain evaluated in this work.

Table 13: Comparison of *G-values* for all types of terrain

	AR	Markov
Proving Ground	1.44E-04	7.64E-06
Unpaved Road	3.46E-02	2.82E-04
U.S. Highway	2.04E-02	2.95E-02

2. Based on the average fatigue lives predicted for the front LCA of the Volkswagen Jetta, it was seen that both the AR and Markov models were successful in generating profiles that contained fatigue-inducing content that matched that of the measured profiles, to within the acceptable limit (i.e. within a factor of 5). However, the values for the AR-synthesised profiles correlated more closely with the values for the measured profiles, as compared to the values for the Markov-synthesised profiles, indicating that the AR model performed better in this regard. Moreover, it was seen that the Markov chain model was not successful at capturing the low frequency content of certain types of terrain. This could be due to the method that was employed to discretise the terrain profile into states. Table 14 shows a comparison of average fatigue lives predicted for the terrain data evaluated in this work.

Table 14: Comparison of average fatigue lives calculated for all types of terrain

	Measured	AR	Markov
Proving Ground	6.979E+02	9.698E+02	2.331E+03
Unpaved Road	2.423E+04	7.028E+03	1.691E+07
U.S. Highway	6.554E+07	5.797E+07	9.912E+06

3. From the spectral density of the measured and synthesised profile, it was seen that both models were successful in capturing the spectral properties of the measured profiles, suggesting that both models performed satisfactorily in this regard.

5.2 Implications of Research

The work presented in this thesis has resulted in a potentially powerful tool for vehicle designers in their attempts to closely correlate computer simulations of vehicle dynamics and reliability with physical tests. The terrain models that have been implemented and tested in this work have been demonstrated to be capable of capturing vehicle excitation properties of certain types of terrain to within reasonable accuracy (i.e. fatigue live correlation to within an order of magnitude). These models can be used to generate synthetic terrain profiles of any desired type, of any desired length, having vehicle excitation content closely conforming to that of measured terrain.

The statistical tests presented in this work afford good insight into the statistical properties of time series data pertinent to terrain modelling. These tests have been utilised to provide information about terrain profiles at different scales, by analyzing the profiles both as a whole, and in discrete 15 m segments.

This analysis capability can be leveraged to characterise different terrain types in terms of their statistical properties. Some of the different terrain types identified for data collection and analysis are:

- Off-road trails
- Asphalt highways
- Concrete highways
- Gravel roads
- City roads

This characterisation will prove useful in specifying requirements for synthesised terrain in virtual vehicle design and development. For example, city roads may be characterised by a certain distribution of statistical metrics. They may be further

classified as ‘smooth’ or ‘rough’ by observing the distribution of their IRI and rainflow count, for example. This capability to simulate terrain based on the particular needs of the user will have significant implications in ground vehicle reliability simulations and towards the development of virtual proving grounds for vehicle design. Vehicle designers will be able to develop virtual driving cycles for durability testing depending on the target vehicle’s requirements. For example, driving cycles generated for sedans can be predominantly pavement based, while those for SUVs and trucks can include portions of off-road trails. These driving cycles may be synthesised using the terrain models implemented in this work, using short sections of measured terrain of each type.

Thus, vehicle engineers will have the ability to develop virtual vehicle driving cycles which will have physical characteristics that match those of existing datasets, while introducing an element of uncertainty and randomness which is required to simulate real world loading characteristics. This capability has significant implications especially in the field of predicting durability and fatigue strength of chassis and suspension components of ground vehicles. Accurately modeled synthetic terrain profiles would allow designers to simulate vehicle excitation which closely represents real world loading conditions, leading to more robust estimation of the service life of automotive components. Additionally, the statistical analysis capability described in this work can prove useful in pavement health monitoring, since the properties of the pavement surface can be evaluated and studied at a local as well as a global level, as it degrades over time.

Researchers can utilise the software application developed as a part of this work, in order to assess the performance of different terrain models for their particular applications. The methodology of quantitatively assessing the performance of terrain models using statistical analysis and fatigue analysis developed in this work can be used to serve as the basis for creating a standardised recommended practice for the usage of terrain models for modelling different types of terrain.

5.3 Discussion & Future Work

5.3.1 Accuracy of terrain data

The statistical measures developed in this work all depend on the quality of the measured profile being analyzed. That is, the ability to model the profile accurately cannot be separated from the accuracy of the original data. Although outside the scope of this work, it is assumed that the accuracy of the profiles being analyzed are consistent with the abilities of current measurement systems. The sampling rate of terrain measurement and the signal processing performed is left to the discretion of the individual researcher. It may be noted that a Class 1 profilometer is one that can sample terrain at intervals below 250 mm with a precision of less than 0.5 mm, while a Class 2 profilometer is one that samples terrain at intervals of up to 500 mm with a precision of below 1 mm [45]. For inertial profiling systems, guidelines for terrain measurement systems can be found in ASTM E950 [46].

5.3.2 Two wheel path representation

If the measured data contains separate profiles for left and right wheel paths, a synthesised profile consisting of two wheel paths can be synthesised as well. This has been done by formulating separate models (AR or Markov) for terrain elevation and bank angle, where each of these are considered to be a series of data points representing elevation and bank angle (both are calculated for every pair of data points as shown in Figure 46). In this way, the correlation between left and right wheel paths may not exist in the transformed data, the elevation and bank angle. Correlation between elevation and bank angle would imply, for example, that as roads rise they typically bank to the left, which is inconsistent with common experience. In Figure 46, the left and right wheel path profiles are shown, along with the bank angle vectors for the 1^{st}, 25^{th} and 50^{th} data points in the profile (as an example). As such, this is a '3D representation' of terrain, but the manner in which it has been applied is still 2-dimensional in effect.

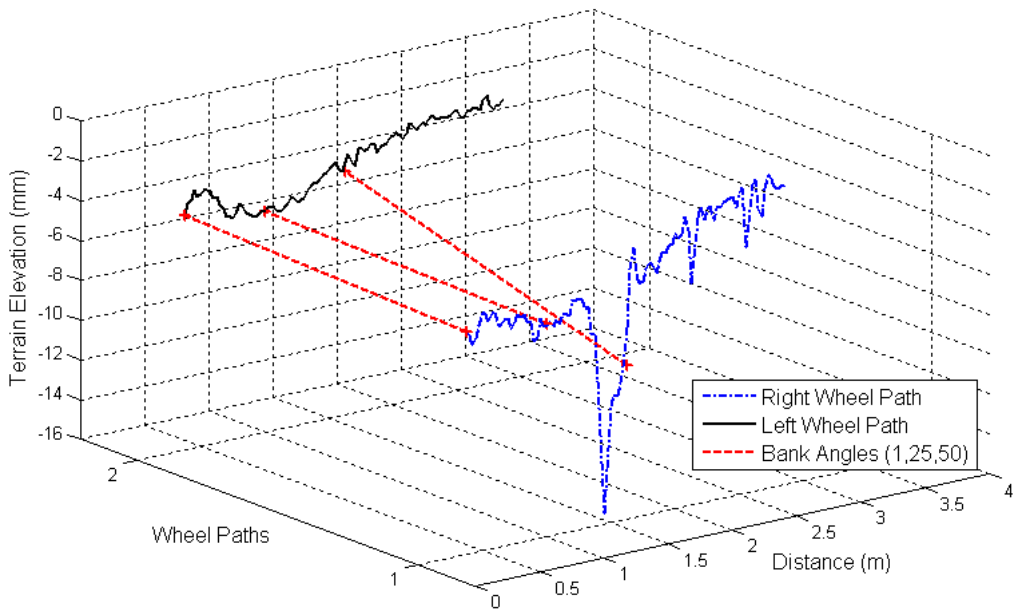

Figure 46: Two wheel path representation

5.3.3 Optimising the AR model parameters

The AR modelling that has been implemented in this work consisted of utilising the coefficients obtained from the measured profile using the Yule-Walker method, for generating synthesised terrain profiles. It is desired to improve the performance of the AR terrain model by optimising these coefficients in order to obtain a terrain profile whose statistical properties closer conform to the measured profile (as well as yield suspension component fatigue lives that closer correlate to those obtained from the measured profile). Initial investigations into implementing a nonlinear optimisation routine in MATLAB have shown promising results, but it was found that the routine was often unable to converge to a solution. This is mainly due to the fact that the random nature of profile synthesis means that repeatability is only possible for realisations of sufficient length, the analysis of which is computationally expensive.

5.3.4 Developing a 2nd order Markov chain model

The first order Markov chain model implemented in this work was demonstrated to be inadequate in capturing the statistical properties of measured terrain profiles, and at vehicle excitation properties of some types of terrain. The performance of this model may be improved firstly by implementing a more appropriate strategy of discretising the profile into non-uniformly spaced states according to the measured terrain data. The confidence in the estimation of transition probabilities would be increased by choosing a lower spacing between states, in ranges where the number of transitions is small. Also, the model can further be improved by extending its scope to the second order.

5.3.5 Application of terrain models to 3-dimensional terrain

The applicability of these methodologies to 3D terrain data can be addressed in future work. The work presented in [47] describes state-of-the-art research focused on representation of 3D terrain. This paper describes a method of decomposing terrain into its 'principle characteristics' i.e. elevation, bank angle, crowning and rutting, and in conjunction, identifying the component of terrain corresponding to each characteristic. Each component of terrain identifies the magnitude of each principle characteristic along the length of the terrain surface. 3D terrain can then be reconstructed by summing the projection of these principle characteristics onto their respective components of terrain. The statistical methodologies presented in this paper could be used to characterise these four primary components of terrain, and is within the scope of future work in this field.

5.3.6 Statistical evaluation

A sensitivity study should be performed in order to assess the importance of each statistical property that is being analysed. It is expected that for different applications (e.g. ride analysis, durability analysis etc.), the importance of each property will vary. Moreover, the analysis of additional statistical properties such as Ride Number, Full Car Roughness Index etc. should be implemented. The PSDs of the terrain profiles should be further studied and characterised in order to further assess the performance of the terrain models.

References

1. Sayers, M.W. and M.S. Karamihas, *The Little Book of Profiling*. 1998, The Regent of the University of Michigan: Ann Arbor, MI.
2. Kern, J.V. and J.B. Ferris, *Development of a 3-D Vehicle-Terrain Measurement System Part I: Equipment Setup*, in *ISTVS: Innovations in Terrain and Vehicle Systems*. 2007, ISTVS: Fairbanks, AK.
3. Wagner, S.M., et al., *Development of a 3-D Vehicle-Terrain Measurement System Part II: Signal Processing and Validation*, in *ISTVS: Innovations in Terrain and Vehicle Systems*. 2007, ISTVS: Fairbanks, AK.
4. Detweiler, Z.R. and J.B. Ferris, *Interpolation methods for High-fidelity three dimensional terrain surfaces.* Journal of Terramechanics, 2009.
5. Detweiler, Z.R. and J.B. Ferris. *Uniform Grid Spacing for Three Dimensional High Fidelity Terrain Profiles*. in *16th International Conference of the International Society for Terrain-Vehicle Systems*. 2008. Turin, Italy.
6. Shannon Wagner, J.B.F., *Developing Stable Autoregressive Models of Terrain Topology*, in *Int. J. Vehicle Systems and Testing*. 2010.
7. Israel, W.B. and J.B. Ferris. *Developing Markov chain models for road surface simulation*. 2007. Orlando, FL, United States: SPIE, Bellingham WA, WA 98227-0010, United States.
8. Andren, P., *Power spectral density approximations of longitudinal road profiles.* International Journal of Vehicle Design, 2006. **40**(1-3): p. 2-14.
9. Rouillard, V., B. Bruscella, and M.A. Sek, *Classification of Road Surface Profiles.* Journal of Transportation Engineering, 2000. **126**(1): p. 41-45.
10. Rouillard, V. and M.A. Sek, *A statistical model for longitudinal road topography.* Road and Transport Research, 2002. **11**(3): p. 17-23.
11. Rouillard, V., M.A. Sek, and B. Bruscella, *Simulation of Road Surface Profiles.* Journal of Transportation Engineering, 2001. **127**(3): p. 247-253.
12. Bruscella, B. and V. Rouillard, *Analysis of Road Surface Profiles.* Journal of Transportation Engineering, 1999. **125**(1): p. 55.
13. Múčka, P. and O. Kropáč, *Simulation of Obstacles in a Longitudinal Road Profile Based on the Weibull Distribution.* Journal of Testing and Evaluation, 2011. **39**(3).
14. Bogsjö, K. and A. Forsan, *Fatigue relevant road surface statistics.* Vehicle System Dynamics, 2004. **41**: p. 724-733.
15. Bogsjö, K., *Development of analysis tools and stochastic models of road profiles regarding their influence on heavy vehicle fatigue.* Vehicle System Dynamics, 2006. **44**: p. 780-790.
16. Kern, J.V., et al. *Characterizing 2D road profiles using ARIMA modeling techniques*. in *Modeling and Simulation for Military Operations II* 2007. Orlando, FL, United States: SPIE, Bellingham WA, WA 98227-0010, United States.
17. Nordberg, T.P., *An iterative approach to road/profile identification utilizing wavelet parameterization.* Vehicle System Dynamics, 2004. **42**(6): p. 413-432.

18. de Pont, J.J. and A. Scott, *Beyond Road Roughness - Interpreting Road Profile Data.* Road and Transport Research, 1999. **8**(1): p. 12-28.
19. Liu Wei, T.F.F., M.ASCE, Zhao Zhe, *Wavelet Analysis and Interpretation of Road Roughness.* Journal of Transportation Engineering,, 2005. **131**(2): p. 120-130.
20. Attoh-Okine, A.Y.A.-P.N.O., *Comparative study of Hilbert-Huang transform, Fourier transform and wavelet transform in pavement profile analysis* Vehicle System Dynamics, 2009. **47**(4): p. 437-456.
21. Sayers, M.W., *Two quarter-car models for defining road roughness. IRI and HRI.* Transportation Research Record, 1989(n 1215): p. 165-172.
22. Sayers, M.W., *On the calculation of international roughness index from longitudinal road profile.* Transportation Research Record, 1995(1501): p. 1-12.
23. Sayers, M.W. and S.M. Karamihas, *Estimation of rideability by analyzing longitudinal road profile.* Transportation Research Record, 1996(1536): p. 110-116.
24. Kropáč, O. and P. Múčka, *Be careful when using the International Roughness Index as an indicator of road unevenness.* Journal of Sound and Vibration, 2005. **287**(4-5): p. 989-1003.
25. Kropáč, O. and P. Múčka, *Alternative single-number indicator of longitudinal road unevenness.* Canadian Journal of Civil Engineering, 2009. **36**(3): p. 389-401.
26. Chaika, M. and D. Gorsich, *Some Statistical Tests in the Study of Terrain Modeling.* International Journal of Vehicle Design, 2004. **36**(2/3): p. 132-148.
27. Redfield, R.C., Karnopp, D. C., *Roadway Elevation Profile Generation for Vehicle Simulation* Vehicle System Dynamics, 1988. **17**(5): p. 267-280.
28. Hammond, J.K. and R.F. Harrison, *Nonstationary response of vehicles on rough ground-a state space approach.* Transactions of the ASME. Journal of Dynamic Systems, Measurement and Control, 1981. **103**(3): p. 245-50.
29. Kern, J.V. and J.B. Ferris. *Characterizing 2-D topographic mappings of roads*. 2006. Chicago, IL, United States: American Society of Mechanical Engineers, New York, NY 10016-5990, United States.
30. Kern, J.V. and J.B. Ferris. *Preliminary Results for Model Identification in Characterizing 2-D Topographic Road Profiles*. in *Proceedings of SPIE - the International Society for Optical Engineering*. 2006. Orlando, Florida.
31. Gorsich, D.J., et al. *Terrain Roughness Standards for Mobility and Ultra-Reliability Prediction*. in *SAE World Congress & Exhibition*. 2003. Detroit, MI.
32. Rouillard, V., B. Bruscella, and M. Sek, *Classification of Road Surface Profiles.* Journal of Transportation Engineering, 2000. **126**(1): p. 41-45.
33. Wagner S. M., F.J.B., *Residual Analysis of Autoregressive Models of Terrain Topology. Submitted to the Journal of Probabilistic Engineering Mechanics*, 2010.
34. Kaner, H.C., Mohanty, S. G., Lyons, J. C., *Critical values of the Kolmogorov-Smirnov one-sample tests.* Psychological Bulletin, 1980. **88(2)**: p. 498-201.
35. Keenan, D.M., *A Tukey nonadditivity-type test for time series nonlinearity.* Biometrika, 1985. **72**(1): p. 39-44.
36. Mohamed, I., Zaharim, A., Yahya, M. S., *Nonlinearity tests for bilinear time series data.* Jurnal Teknology, 2005. **42(C)**.

37. Chaika, M., D. Gorsich, and T.C. Sun, *Some statistical tests in the study of terrain modelling.* International Journal of Vehicle Design, 2004. **36**(2): p. 132-148.
38. Taylor, H. and S. Karlin, *An Introduction to Stochastic Modeling*. III ed. 1996: Academic Press.
39. Travis W. Beck, T.J.H., Joseph P. Weir , Joel T. Cramer , Vassilios Vardaxis , and J.W.C. Glen O. Johnson , Moh H. Malek , Michelle Mielke, *An examination of the Runs Test, Reverse Arrangements Test, and modified Reverse Arrangements Test for assessing surface EMG signal stationarity.* Journal of Neuroscience Methods, 2006. **156**(1-2): p. 242-248.
40. Brockwell and Davis, *Introduction to Time Series and Forecasting*. 2002: Springer Verlag.
41. Niesłony, A., *Determination of fragments of multiaxial service loading strongly influencing the fatigue of machine components.* Mechanical Systems and Signal Processing, 2009. **23**(8): p. 2712-2721.
42. *ASTM E 1049-85: Standard practices for cycle counting in fatigue analysis*, in *Annual Book of ASTM Standards*. 1999, ASTM. p. 710-718.
43. *Radioss Documentation*. 2007, Altair Engineering.
44. Gokhale, et al., *Practical Finite Element Analysis*. Vol. 1. 2008, Pune, India.
45. Bennett, C.R., *Calibrating Road Roughness Meters in Developing Countries.* Committee on Surface Properties-Vehicle Interaction, 1996.
46. ASTM, *Standard Test Method for Measuring the Longitudinal Profile of Traveled Surfaces with an Accelerometer Establsihed Inertial Profiling Reference*. 2004, ASTM International: West Conshohocken, PA.
47. Chemistruck, H. and J. Ferris, *Compact Models of Terrain Surfaces.* Proceedings of ASME Dynamic Systems and Controls Conference, Boston, MA., 2010.
48. Chemistruck, H., *A Galerkin Approach to Define Measured Terrain Surfaces with Analytic Basis Vectors to Produce a Compact Representation*, in *Mechanical Engineering*. 2010, Virginia Tech.

Appendix A: Curved Regular Grid

Terrain measurement using an advanced profilometer like the VTMS yields a point cloud of terrain height data located in the horizontal plane. A set of longitudinal (to the profilometer body) vectors *u*, and transverse vectors, *v*, are used in order to form a curved regular grid (CRG) in the horizontal plane, as shown in Figure 47. Discrete longitudinal locations along vector *u* are are indexed by *i*, whereas discrete transverse locations along vector *v* are indexed by *j*. The terrain height corresponding to each discrete horizontal grid point (*u*, *v*) is determined by utilising the vertical heights in the localised area around that horizontal location. Various spatial interpolation methods may be used for this purpose (e.g. inverse distance to a power, Kriging etc.). In this way, each terrain surface comprises a sequence of transverse scans, perpendicular to the direction of vehicle travel, that have been nominally corrected for body motion.

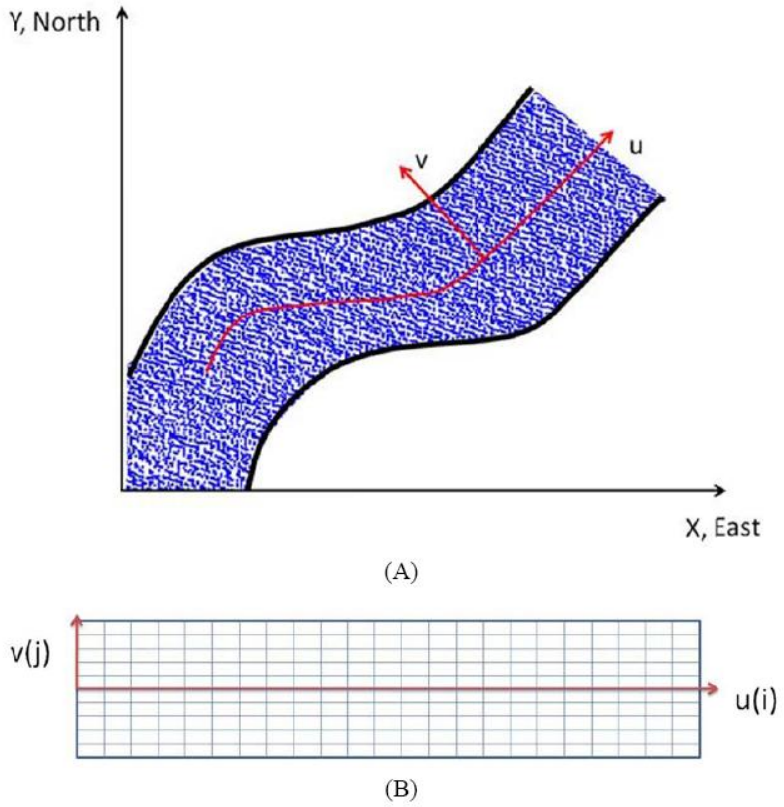

Figure 47: Curved Regular Grid [48]
(a) Point cloud obtained from profilometer
(b) Uniformly gridded format of CRG

Appendix B: Equations for IRI Calculations

$c = c_s / m_s = 6.0$
$k_1 = k_{us} / m_s = 653$
$k_2 = k_s / m_s = 63.3$
$\mu = m_{us} / m_s = 0.15$

$$\sum F_x = m\ddot{x}$$

$$-k_s(x_1 - x_2) - c_s(\dot{x}_1 - \dot{x}_2) = m_s\ddot{x}_1$$
$$m_s\ddot{x}_1 + k_s(x_1 - x_2) + c_s(\dot{x}_1 - \dot{x}_2) = 0$$

$$k_s(x_1 - x_2) + c_s(\dot{x}_1 - \dot{x}_2) - k_{us}(x_2 - h(t)) = m_{us}\ddot{x}_1$$
$$m_{us}\ddot{x}_1 - k_s(x_1 - x_2) - c_s(\dot{x}_1 - \dot{x}_2) + k_{us}x_2 = k_{us}h(t))$$

$$\begin{bmatrix} m_s & 0 \\ 0 & m_{us} \end{bmatrix}\begin{bmatrix} \ddot{x}_1 \\ \ddot{x}_2 \end{bmatrix} + \begin{bmatrix} c_s & -c_s \\ -c_s & c_s \end{bmatrix}\begin{bmatrix} \dot{x}_1 \\ \dot{x}_2 \end{bmatrix} + \begin{bmatrix} k_s & -k_s \\ -k_s & k_s + k_{us} \end{bmatrix}\begin{bmatrix} x_1 \\ x_2 \end{bmatrix} = k_{us}\begin{bmatrix} 0 \\ h(t) \end{bmatrix}$$
$$\begin{bmatrix} 1 & 0 \\ 0 & m_{us}/m_s \end{bmatrix}\begin{bmatrix} \ddot{x}_1 \\ \ddot{x}_2 \end{bmatrix} + \begin{bmatrix} c_s/m_s & -c_s/m_s \\ -c_s/m_s & c_s/m_s \end{bmatrix}\begin{bmatrix} \dot{x}_1 \\ \dot{x}_2 \end{bmatrix} + \begin{bmatrix} k_s/m_s & -k_s/m_s \\ -k_s/m_s & (k_s + k_{us})/m_s \end{bmatrix}\begin{bmatrix} x_1 \\ x_2 \end{bmatrix} = \frac{k_{us}}{m_s}\begin{bmatrix} 0 \\ h(t) \end{bmatrix}$$
$$\begin{bmatrix} 1 & 0 \\ 0 & \mu \end{bmatrix}\begin{bmatrix} \ddot{x}_1 \\ \ddot{x}_2 \end{bmatrix} + \begin{bmatrix} c & -c \\ -c & c \end{bmatrix}\begin{bmatrix} \dot{x}_1 \\ \dot{x}_2 \end{bmatrix} + \begin{bmatrix} k_2 & -k_2 \\ -k_2 & k_2 + k_1 \end{bmatrix}\begin{bmatrix} x_1 \\ x_2 \end{bmatrix} = \begin{bmatrix} 0 \\ k_1 \end{bmatrix}h(t)$$

$$x(t) = \begin{bmatrix} \dot{x}_1 \\ \dot{x}_2 \\ x_1 \\ x_2 \end{bmatrix}$$

$$M = \begin{bmatrix} 1 & 0 \\ 0 & \mu \end{bmatrix}$$

$$C = \begin{bmatrix} c & -c \\ -c & c \end{bmatrix}$$

$$K = \begin{bmatrix} k_2 & -k_2 \\ -k_2 & k_2 + k_1 \end{bmatrix}$$

$$F = \begin{bmatrix} 0 \\ 0 \\ 0 \\ k_1 \end{bmatrix}h(t)$$

$$A = \begin{bmatrix} 0 & I \\ M^{-1}K & M^{-1}C \end{bmatrix}$$

$$B = M^{-1}F$$

$$\dot{x} = Ax + B$$

$$IRI = \frac{1}{L}\int_{0}^{L/V} \left|\dot{x}_1 - \dot{x}_2\right| dt$$